QUANTITATIVE NON-DESTRUCTIVE CHARACTERIZATION OF DEFECTS IN ELECTRONIC PACKAGES USING FUZZY INFERENCE BASED THERMAL TOMOGRAPHY

by

Çağdaş Muratoğlu

B.S., Mechanical Engineering, Boğaziçi University, 2018

Submitted to the Institute for Graduate Studies in
Science and Engineering in partial fulfillment of
the requirements for the degree of
Master of Science

Graduate Program in Mechanical Engineering
Boğaziçi University
2022

ACKNOWLEDGEMENTS

Firstly, I would like to express my deepest gratitude to my thesis supervisor, Prof. Hakan Ertürk, for his patience, support, and the precious knowledge he shared with me. It was a great honor for me to have the chance to work with him.

I would also like to express my gratitude and love to my family. They have always supported and encouraged me during my 3 years long bumpy road of thesis study. I am also grateful to TÜBİTAK for supporting me financially during my study.

Once and for all, I would like to dedicate this thesis to my love and my best friend, Duygu, for her deep understanding, unconditional compassion, and wholehearted support through those tough days.

ABSTRACT

QUANTITATIVE NON-DESTRUCTIVE CHARACTERIZATION OF DEFECTS IN ELECTRONIC PACKAGES USING FUZZY INFERENCE BASED THERMAL TOMOGRAPHY

Thermal challenges have been a roadblock for electronic packaging with the increasing number of transistors and smaller package sizes. Thermal interface material (TIM) layers play a key role in heat dissipation at all levels within an electronic package. The function of TIM is to minimize the thermal contact resistance by filling the microscale gaps between the die and the integrated heat spreader (IHS). For this reason, there have been intensive efforts to achieve a high-quality TIM in electronic packaging. Defects in TIM layers must be identified during the assembly process development to obtain dependable thermal management. Non-destructive characterization techniques such as scanning acoustic microscopy or X-ray tomography have been used to identify such defects and help to advance manufacturing procedures. Thermal tomography is proposed as a low-cost alternative to these qualitative imaging techniques, all of which require high-cost devices and a long processing time. The location and size of defects are identified by evaluating the measured thermal response of a heated electronic package. Fuzzy inference method (FIM) is used as an image reconstruction algorithm to solve the resulting ill-posed inverse problem. The feasibility of thermal tomography is studied numerically; therefore, simulated measurements are used in this study rather than experimental data. The results indicate that the fuzzy inference based thermal tomography can be a powerful tool for quantitative non-destructive characterization of defects in the electronic packages, with less cost and shorter processing time than other established methods.

ÖZET

ELEKTRONİK PAKETLERDEKİ KUSURLARIN BULANIK ÇIKARIM TABANLI ISIL GÖRÜNTÜLEME KULLANILARAK NİCELİKSEL TAHRİBATSIZ MUAYENESİ

Isıl zorluklar, artan transistör sayısı ve daha küçük paket boyutları ile elektronik paketleme için bir engel teşkil etmektedir. Isıl arayüz malzemesi katmanları, bir elektronik paket içindeki tüm seviyelerde ısı dağılımında önemli bir rol oynar. Isıl arayüz malzemelerinin işlevi, çip ve birleştirilmiş ısı dağıtıcı arasındaki mikro ölçekli boşlukları doldurarak ısıl temas direncini en aza indirmektir. Bu nedenle elektronik paketlemede yüksek kaliteli bir ısıl arayüz malzemesi elde etmek için yoğun çaba sarf edilmektedir. Güvenilir ısıl yönetim elde etmek için ısıl arayüz malzemesi katmanlarındaki kusurlar, montaj süreci geliştirme sırasında tanımlanmalıdır. Bu tür kusurları belirlemek ve üretim prosedürlerini geliştirmek için taramalı akustik mikroskopi veya X-ışını tomografisi gibi tahribatsız muayene teknikleri kullanılmıştır. Isıl görüntüleme, tümü yüksek fiyatlı cihazlar ve uzun işlem süresi gerektiren bu niteliksel görüntüleme tekniklerine düşük maliyetli bir alternatif olarak önerilmektedir. Kusurların yeri ve boyutu, ısıtılmış bir elektronik paketin ölçülen ısıl tepkisi değerlendirilerek tanımlanır. Bulanık çıkarım yöntemi, ortaya çıkan kötü konumlanmış ters problemi çözmek için bir görüntü yeniden yapılandırma algoritması olarak kullanılır. Isıl görüntülemenin uygulanabilirliği sayısal olarak incelenmektedir; bu nedenle, bu çalışmada deneysel veriler yerine simüle edilmiş ölçümler kullanılmıştır. Sonuçlar, bulanık çıkarım tabanlı ısıl görüntülemenin, elektronik paketlerdeki kusurların niceliksel tahribatsız muayenesi için, diğer yerleşik yöntemlere kıyasla daha az maliyet ve daha kısa işlem süresi ile güçlü bir araç olabileceğini göstermektedir.

TABLE OF CONTENTS

LIST OF FIGURES

LIST OF TABLES

LIST OF SYMBOLS

C	Volumetric heat capacity
c_p	Specific heat capacity
e_m	Average of temperature deviations at mth measurement point
$e_{m,s}$	Temperature deviation at mth point for sth time
g	gth sub volume
G	Total number of sub volumes
h_{eff}	Effective heat transfer coefficient
J	Objective function
k	Thermal conductivity
L_x	Length along the x-axis
L_y	Length along the y-axis
L_z	Length along the z-axis
m	mth temperature measurement point
M	Total number of temperature measurement point
n	Number of iteration
p_e	Domain of the e_m
p_e	Domain of the Δu_m
q''	Heat flux
q^{exa}	Exact distributed heat flux
$\boldsymbol{r}$	Coordinate vector
s	sth temperature measurement time
S	Total number of temperature measurement time
t	Time
T	Temperature
T_j	Junction temperature
$T_{m,s}^{cal}$	Calculated temperature at mth point for sth time
$T_{m,s}^{mea}$	Measured temperature at mth point for sth time
T_∞	Ambient temperature

V_v	Volume of the void in a control volume
V	Control volume
$\alpha_{g,m}$	Weighting coefficient
γ_{A_l}	Membership degree of input variable
γ_{B_l}	Membership degree of output variable
Δu_m	Fuzzy inference result at mth point
$\Delta\varphi$	Adjustment vector for void fractions
$\mathcal{E}$	Convergence criteria
θ_1	Variation coefficient for the x-direction
θ_2	Variation coefficient for the y-direction
θ_3	Variation coefficient for the z-direction
ρ	Density
σ	Standard deviation
φ	Void fraction in TIM

LIST OF ACRONYMS/ABBREVIATIONS

CGM	Conjugate Gradient Method
DFI	Decentralized Fuzzy Inference
DDFI	Double Decentralized Fuzzy Inference
FIM	Fuzzy Inference Method
FIU	Fuzzy Inference Units
GA	Genetic Algorithm
GCI	Grid Convergence Index
IC	Integrated Circuit
IHCP	Inverse Heat Conduction Problem
IHS	Integrated Heat Spreader
IHTP	Inverse Heat Transfer Problem
IR	Infrared
L-MM	Levenberg-Marquardt Method
NB	Negative Big
NDT	Non-Destructive Testing
NM	Negative Medium
NS	Negative Small
PB	Positive Big
PM	Positive Medium
PS	Positive Small
SAM	Scanning Acoustic Microscopy
SDM	Steepest Descent Method
TIM	Thermal Interface Material
ZO	Zero

1. INTRODUCTION

1.1. Problem Overview

The electronics industry has been following "Moore's Law", a projection or forecast proved to be valid for the past fifty years. The law states that the number of transistors in an integrated circuit (IC) approximately doubles every two years, and it has been a reliable predictor of the speed of electronic technology advancement since 1965 [1]. Today there are millions of transistors on a single IC chip, providing enormous computing power. However, severe limitations may restrict further electronic miniaturization and growing computing power.

One of the most significant limitations that have been encountered is thermal management. Although it was once thought that the chips would be faster and consume less power when they scaled to smaller sizes, they overheat as electrons moved faster through smaller silicon circuits below 90 nanometers. The industry embraced an integrated solution to overcome thermal management problems, including package level management, component level cooling solutions, improving transistor architecture, manufacturing process, and chip design.

The electronic package serves as a connection between the die (chip) and the motherboard to obtain a solid performance in power and signal delivery, heat dissipation, and protection from mechanical damage. Thermal interface material (TIM) layers are placed among different package layers to reduce thermal contact resistance and improve heat removal from the package.

A thermal resistance is observed at the interface when two solid layers are in contact, depending on the pressure used to hold them together and the micro-scale roughness over the facing surfaces. Another layer is usually added as a filler to reduce the thermal contact resistance, in which case the characteristics of the layer are crucial.

In flip chip packages, which are predominantly used for central processing units of high-performance computers, a TIM layer referred to as TIM1 is inserted between the die and integrated heat spreader (IHS), and another layer referred to as TIM2 is inserted between the IHS and heat sink as an interface layer. Thus, the characteristics of TIM layers are essential for achieving the required cooling performance [2].

Thermally conductive elastomers, phase change materials, thermally conductive adhesive tapes and solders are the most common thermal interface materials [3]. The application of the TIM1 layer during the assembly process is cumbersome as they can have defects such as dendrite growth, metal migration, interfacial delamination, micro-cracks, and voids [4, 5]. It is desired to prevent such defect formations as they lead to poor thermal performance.

Electronic package assembly process development aims to determine the optimum parameters that provide the best mechanical, electrical, and thermal performance. In accordance with this purpose, a large number of prototype packages, generally referred to as "test vehicles", are manufactured and tested to optimize process parameters.

Thermal test is one of the tests performed on the test vehicles, which evaluates the package's thermal resistance. Thermal resistance of the package is identified from the highest temperature of the die, junction temperature, to the upper surface temperature of the lid, case temperature. When the measured thermal resistance is higher than the desired one, the package must have a defect to be identified to achieve a high-quality interface layer by modifying the assembly process. Therefore, the non-destructive characterization of defects within TIM plays a crucial role in the assembly process development. In particular, defects within TIM1 are more significant because a 20% void in TIM2 increases the package's thermal resistance by 10%, while a same-sized void in TIM1 will increase it by 250% [6].

Various non-destructive testing (NDT) techniques are used for defect characterization in electronic packages. These include atomic force microscope, optical microscope, magnetic microscopy, scanning acoustic microscopy (SAM), X-ray, and liquid crystal thermography. In recent years, infrared (IR) imaging has been introduced as an practical way of inspecting defects that produce thermal failure in TIM [5, 7, 8]. IR imaging evaluates the temperature response of the system to the performed heat flux to discover the defected area qualitatively relying on an IR camera. While these qualitative approaches should be regarded as complementary solutions, quantitative characterization of defects is also possible and has been investigated by researchers lately.

Thermal tomography is a thermal characterization technique that uses a thermal signal diffusing through the characterized object, and the characterization is based on an IR image of an area. Unknown parameters are estimated using temperature measurement data and image reconstruction algorithms. Thus, defects can be characterized by estimated parameters which are material properties in this case.

The implementation of thermal tomography for quantitative defect characterization in electronic packages faces three major challenges. First, the spreading effect due to different IHS and die sizes leads to the loss of thermal signal. Second, estimating material properties from temperature measurement data constitutes an inverse problem that is typically ill-posed, and the solutions' existence, stability, and uniqueness might not be all satisfied. Therefore, the image reconstruction algorithm used must be able to overcome these challenges. Lastly, there is a practical difficulty associated with powering the die for a very short time as the heat sink is removed to capture thermal images.

1.2. Literature Survey

1.2.1. Non-destructive Testing Techniques

X-ray imaging is one of the earliest methods in IC package inspection [9]. An X-ray is sent from a source to a receiver, based on interaction of X-ray photons with the package and signal received by a detector, an image of package is constructed reflecting the elemental composition of the material and and the geometry of the package. Defects in the package can be observed from the images qualitatively [10], or quantitative data can be generated with the help of image processing tools.

Scanning acoustic microscopy creates visual images of differences in the mechanical characteristics of an electronic package by using acoustic waves as a source. The transducer, which transforms electrical signals into acoustic signals, is the essential component of an acoustic microscope. The acoustic waves are focused and transmitted to the package via a couplant, usually distilled water or alcohol. The couplant conveys an effective ultrasonic propagation to the electronic package in this case. When the emitted acoustic waves interact with the package, part of the waves reflect to the transducer while others are transmitted [11]. Defects such as delaminations and voids lead to air gaps, and ultrasound cannot travel through the air, leading to the identification of the defect [12].

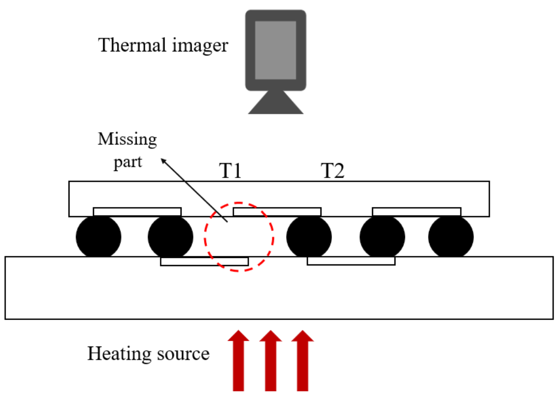

Figure 1.1. Schematic image of an example IR imaging inspection for IC packaging.

Infrared imaging is one of the most widely used NDT technologies for material assessment. The IR imaging method's primary operating premise is to detect the emission from the surface within IR wavelengths and capture the surface's temperature distribution [13]. The IR imaging method has been used to inspect IC packaging for almost half a century [14,15], and it has become a practical NDT technique to examine electronic packaging since then [5, 16–18]. Either the die is powered up or an external heat flux is applied to evaluate the temperature response at the top surface of IHS via an IR camera. Heat penetrates the IC package over time, while subsurface defects alter heat flow. In this way, IR imaging can qualitatively detect defects in the IC package. The schematic diagram of an example IR imaging method is illustrated in Figure 1.1.

These above-mentioned non-destructive techniques produce qualitative outcomes, and they should be considered complementary solutions. X-ray inspection is promising to detect voids with a resolution at the micron level, and it is suitable for an in-line application. However, it has a long processing time in the order of hours [10]. SAM inspection has poor sensitivity to edge defects due to the so-called edge effect, which is the distortion of reflections from the edge [19]. Also, it is not convenient for an in-line application. The benefits of IR imaging are ease of setup procedure, its direct relation to thermal behavior, and rapid application for extensive area assessment. Nevertheless, the defect image acquired by IR imaging might not be totally apparent because of lateral heat dissipation [17].

Thermal tomography is a thermal imaging method that uses a thermal signal that diffuses through the characterized object and allows qualitative and quantitative examination. Previous studies revealed that thermal tomography is suitable for fast, comprehensive, and low-cost detection [2, 20], and it can be used for medical [21] and materials science [22, 23] applications. Even though thermal diffusion rate can restrain the precision of defect characterization, research on the quantitative non-destructive characterization of defects using thermal tomography is still progressing [24].

Thermal tomography can be implemented coupled with IR imaging in electronic packaging. The test vehicle is heated either by providing power to die or applying an external heat flux. Then the temperature data can be taken by high-speed IR cameras from the top of the surface. These temperature measurements are used in image reconstruction algorithms to estimate the unknown material properties, which characterize defects in electronic packaging.

1.2.2. Algorithms to Solve Inverse Heat Transfer Problems

Thermal tomography technique typically involves a problem classified as an inverse heat transfer problem (IHTP). Direct heat transfer problems are primarily concerned with determining the temperature distribution when the initial and boundary conditions, heat generation rates, and thermophysical properties are known. In opposition to direct heat transfer problems, IHTPs are concerned with estimating the unknown characteristic parameters such as boundary conditions, heat generation, and thermophysical properties by using internal or surface temperature measurements. Direct heat transfer problems are mathematically classified as well-posed, as the conditions of existence, stability, and uniqueness are all satisfied for their solutions with the input data. On the other hand, IHTPs are typically ill-posed, which means that the solutions' existence, stability, and uniqueness might not be all satisfied.

While the existence of a solution for an IHTP can be ensured, the uniqueness condition can be mathematically proven only for some particular instances. However, the unavoidable random errors (noise) in the measurements might induce a dramatic change in the estimated unknowns leading to issues related to stability. As a result, specific approaches are necessary to handle the stability issues for an IHTP solution [25].

Inverse heat transfer problems can be classified according to the mode of heat transfer; conduction, convection, radiation, or a combination of these. An alternative categorization considers the estimated parameter in the problem; boundary condition estimation problems, initial condition estimation problems, source estimation problems, geometry estimation problems, and material property estimation problems. Conduction is the primary heat transfer mechanism in the thermal tomography problem presented here, and the resulting inverse heat conduction problem (IHCP) is about estimating the thermal properties of a material in this study.

Inverse heat conduction studies started in the late 1950s with the pioneering engineering work by Shumakov [26] in the Soviet Union. It became known in the USA by the work published by Stolz [27] in 1960. For years, the IHCPs were assumed to be insolvable, or the outcomes were considered to be meaningless when any of the conditions mentioned above were not satisfied. Thus, there was a loss of interest among engineers, physicists, and mathematicians for the solution of IHCPs [28]. It was Tikhonov's regularization technique [29,30], Alifanov's iterative regularization methods [28, 31], and Beck's parameter estimation [32] approach that showed the solution of IHCPs possible.

With the availability of high speed and large capacity computers, many scholars have proposed various new techniques for a successful solution of IHCPs during the last decades. Regarding the defect characterization, Siavashi *et al.* [33] applied the conjugate gradient method (CGM) to spot the two-dimensional flaws with various geometries and sizes in a specimen under the steady-state heat conduction. They analyzed the effect of the initial guesses and the number of measurement points on the defect characterization.

Huang and Chaing [34] used the steepest descent method (SDM) in a three-dimensional thermal tomography problem to characterize the shape of the unknown surface. Three test cases are used to evaluate the validity of thermal tomography, each with a different initial guess and measurement error. Fan *et al.* [35] utilized the Levenberg-Marquardt method (L-MM) to specify the size, depth and thermal conductivity of a subsurface defect, and the influence of the measurement errors, defect depth, and material's thermal conductivity on the defect characterization results.

Ertürk [24] evaluated the iterative perturbation method, Levenberg-Marquardt, and Regularized Newton-Gauss algorithms for non-destructive characterization of thermal interfaces for electronic packages. It is shown that all three methods can estimate the void distribution within the thermal interface, and if the number of measurements taken at different times is high enough, all three algorithms' prediction accuracy, convergence rate, and computational effort are comparable. The study uses a simplistic geometry in which the heat spreading effect is not considered.

Öner and Ertürk [36] investigated the feasibility of thermal tomography for an electronic package, where the spreading effect is considered due to different sized IHS and die. The study aims to identify defects in TIM quantitatively by detecting void location and size following the formulation outlined by Ertürk [24]. Öner and Ertürk [36] used L-MM as an image reconstruction algorithm to solve the resulting IHCP. The results show that the method is useful to identify defects causing more significant temperature differences in the thermal performance test. However, the study has limited resolution for void fractions due to L-MM's computationally expensive calculation of Jacobian matrix that shows the effect of change in void fraction distribution on the temperature distribution of the system. Therefore, the Jacobian size increases quadratically as finer resolution grids are selected, leading to a higher computation time.

Besides widely used gradient-based optimization algorithms, some metaheuristics for solving IHCPs are also available in the literature. Divo *et al.* [37] employed genetic algorithm (GA) to specify the subsurface defects in a two-dimensional heat-conducting specimen using the temperature measurements from the IR image. Genetic algorithm is a global search algorithm, and the main drawback of this technique is its long computation time during the search process. For a three-dimensional problem, this shortcoming will be more significant. Kou *et al.* [38] applied a bacterial colony chemotaxis algorithm and the radial basis function neural network to identify the defect parameters. The accuracy of characterization depends mainly on a significant quantity of experimental data, and the adaptability of this method is not decisive.

One of the more recent methods for handling ill-posed IHCPs is fuzzy inference method (FIM) presented by Wang *et al.* [39], which is an approach based on fuzzy logic theory. The results show that FIM can successfully estimate the unknown parameters and effectively reduce dependency on the number of measurement points, initial guesses, and temperature measurement errors. Also, this method does not use the Jacobian matrix to calculate the effect of the change in void fraction distribution on the temperature distribution of the system.

1.2.3. Fuzzy Inference Method

Fuzzy logic is a form of many-valued logic in which the truth value of variables range between 0 and 1, contrasting with traditional Boolean logic. It is used to deal with the concept of partial truth, in which the truth value may range between completely true and completely false. Fuzzy logic was introduced by Lotfi Zadeh [40] in 1965, and it arises from the observation that people can make decisions based on imprecise and non-numerical knowledge. Fuzzy models are mathematical means of referring to ambiguity and imprecise information, as it can be understood from the word fuzzy. These models are capable of recognizing, representing, processing, interpreting, and utilizing data that are ambiguous and contain uncertainty.

Fuzzy inference is a method that interprets the values in the input vector and assigns values to the output vector based on specific sets of rules relating quantitative information to qualitative. Fuzzy inference systems have been successfully performed in several engineering fields, such as automatic control, data classification, and decision analysis [41]. However, its application in inverse heat conduction studies is quite limited.

Wang *et al.* [39] used fuzzy inference process to estimate the unknown boundary condition of an IHCP. A decentralized fuzzy inference (DFI) method is used for the two-dimensional steady IHCP, where the finite difference method is used to model heat conduction. The results are compared with those predicted by L-MM. The comparison shows that the DFI method has higher prediction accuracy than L-MM when there are few measurement points, poor initial guesses, and large temperature measurement errors.

Although the finite difference method and the finite element method are widely used discretization approaches for modeling, their mesh-dependent characteristics require substantial computational effort when a high number of grids are needed. Li *et al.* [42] used the DFI method to solve an IHCP using the boundary element method for modeling, transforming heat conduction equations into boundary integral equations to prevent this issue. The boundary element method only discretizes the system boundary, which reduces the computation time required for the solution of the direct problem. The results predicted by DFI are compared with those predicted by CGM. The outcome is similar to the previous study regarding the dependency on the number of measurement points, initial guesses, and temperature measurement errors.

Wang *et al.* [43] proposed a double decentralized fuzzy inference (DDFI) method to estimate time-dependent unknown boundary conditions. A two-dimensional transient IHCP is solved, and the results are compared with the dynamic matrix control method. The study shows that the DDFI method predicts more accurately than the dynamic matrix control method when there are large temperature measurement errors.

After two-dimensional and transient IHCPs, Wang *et al.* [44] used the DFI method to solve a three-dimensional steady-state IHCP. The impacts of different functional forms of the heat flux distribution, initial condition guesses, and measurement errors are also observed and compared with CGM. The DFI method has higher prediction accuracy than CGM when there are few measurement points, poor initial guesses, and large temperature measurement errors.

The most recent study using the fuzzy inference method to identify a three-dimensional subsurface defect is by Wang *et al.* [45]. The problem is solved using the finite element method. It is simply a steady-state conducting cuboid specimen with a three-dimensional subsurface defect. The effects of the defect size and shape, the initial guess value, the number of measurement points, and the temperature measurement errors on the characterization results are studied and compared with L-MM. The results show that the prediction accuracy of FIM depends less on the factors mentioned above, with fewer iterations and less computation time.

1.3. Objective

Various NDT techniques such as X-ray and SAM are used for defect characterization in electronic packages. These qualitative approaches are promising to detect voids with a resolution at the micron level. However, they require high-cost devices and a long processing time. Thermal tomography is proposed as a low-cost and rapid alternative to these qualitative approaches and allows qualitative and quantitative examination. Thermal tomography is performed on a flip chip electronic package in which the spreading effect is considered due to different sized IHS and die in this study. The package is heated by applying power to the die, and the measured response is the temperature distribution obtained by temporal IR camera readings from the top surface of IHS. The objective of this study is to quantitatively identify defects in TIM by detecting void location and size. The fuzzy inference method is proposed to solve the resulting inverse problem because it does not include computationally expensive calculation of Jacobian matrix, and it is expected to detect smaller voids by reaching higher grid resolution than similar studies.

2. PROBLEM DESCRIPTION AND FORMULATION

2.1. Problem Description

As mentioned earlier, a large number of packages are produced and tested to identify optimum process parameters during the assembly process development. A flip chip electronic package with an air-cooled heat sink used for a thermal performance test is shown in Figure 2.1. If the measured thermal resistance of the package is higher than the targeted specification during the test, the package is assumed to have a defect to be identified, and the problem in the process must be identified and fixed.

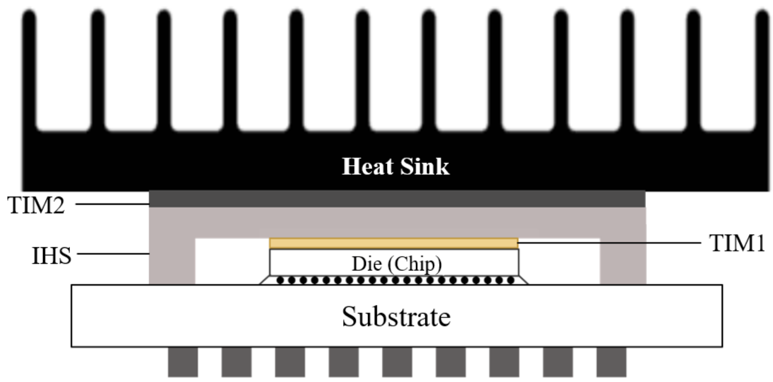

Figure 2.1. A standard electronic package used in regular development test (Test-1).

Qualitative methods such as X-ray and SAM are used to determine defects in the interface layer during process development. As it is proposed to identify defects quantitatively using thermal tomography, another test is performed on the package, as shown in Figure 2.2.

Thermal tomography test (Test-2) consists of two simultaneous steps: heating the package with no cooling solutions attached and recording the thermal image over the IHS surface using an IR camera. A constant uniform die power of 90 W is applied for 100 ms to heat the package, and the heat sink used in the standard electronic package is removed to capture IR images. Instead, the air moved by a fan is directed over the IHS to provide cooling, with an effective heat transfer coefficient (h_{eff}) of 100 W/(m^2 K) that is typical for forced convection of air. Thermal images of the IHS top surface are recorded with 10 ms intervals during 100 ms of heating. These images are utilized to characterize TIM1 layer using a fuzzy inference algorithm.

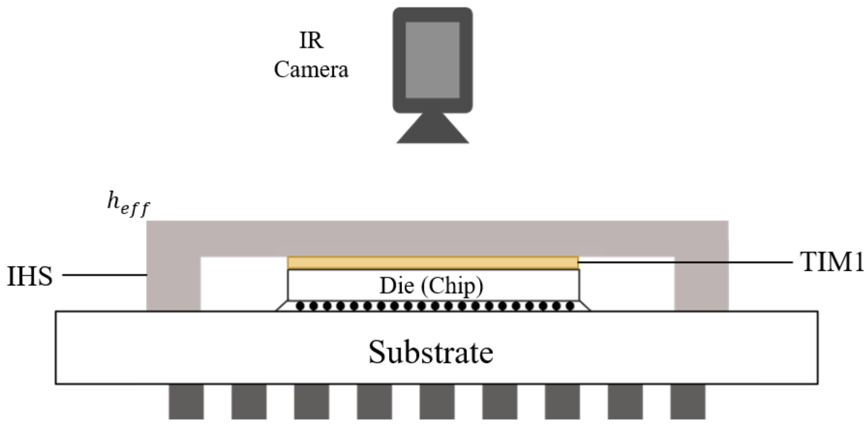

Figure 2.2. An electronic package used in thermal tomography (Test-2).

This study aims to introduce the concept theoretically, utilizing numerical simulations rather than experiments. The simplified geometry of electronic package in thermal performance test (Test-1) and in thermal tomography test (Test-2) with the boundary conditions considered are shown in Figure 2.3 and Figure 2.4, respectively.

In Test-1, the heat sink is modeled only with its base, and an effective heat transfer coefficient (h_{eff}) of 1600 W/(m^2 K) is applied that represents the effect of a typical heat sink. A constant uniform die power of 90 W is applied until the system reaches steady state. The ambient temperature is considered to be 20 °C in both tests. Dimensions and thermophysical properties of the package components [46] are shown in Table 2.1 where k is thermal conductivity, ρ is density, and c_p is specific heat capacity.

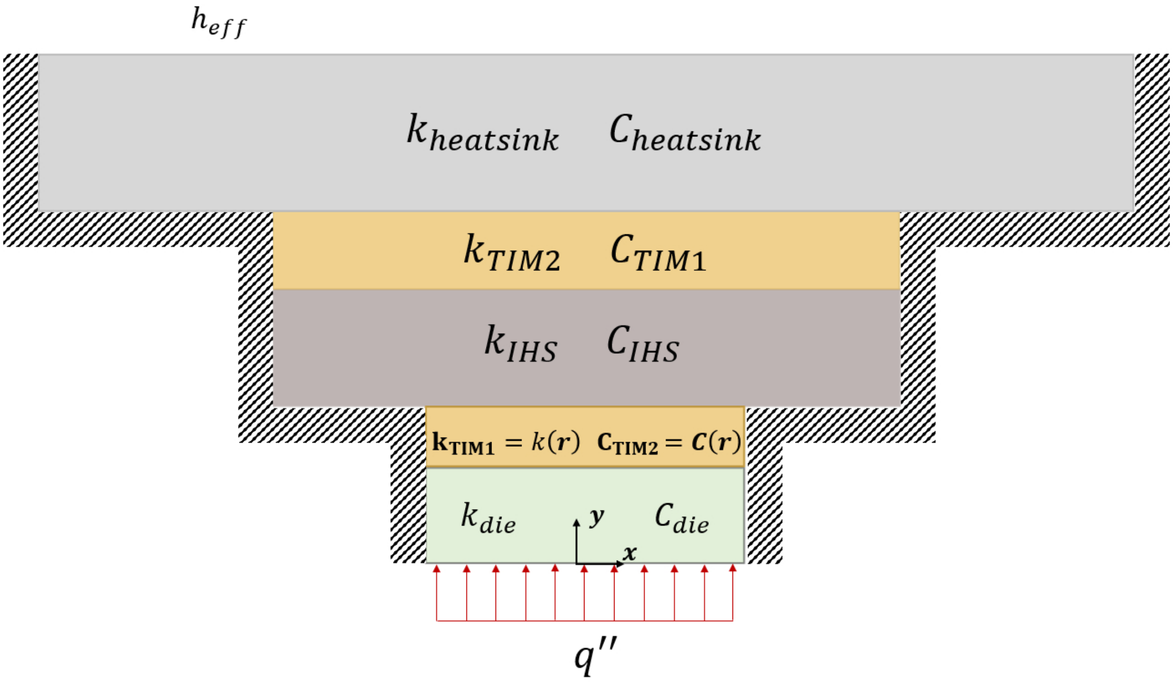

Figure 2.3. Simplified geometry of electronic package in Test-1 (shown in two dimensions, not to scale).

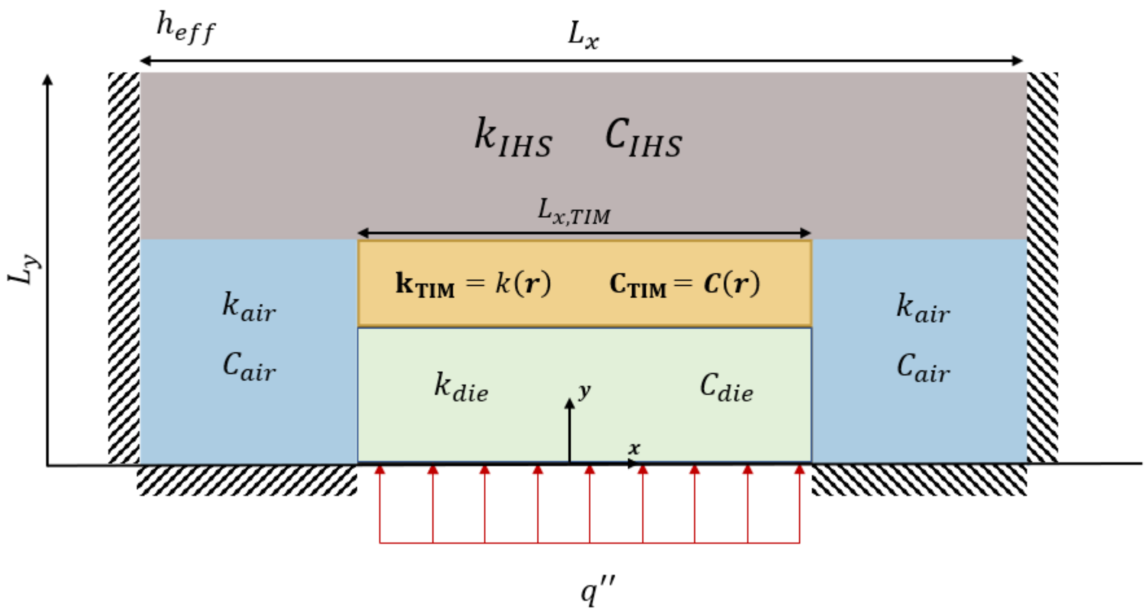

Figure 2.4. Simplified geometry of electronic package in Test-2 (shown in two dimensions, not to scale).

Table 2.1. Dimensions and thermophysical properties of the package components.

Component	**Material**	**Dimensions** [mm^3]	k [W/m-K]	ρ [kg/m^3]	c_p [J/kg-K]
Die	Silicon	10x10x0.55	141.2	2330	700
TIM1	G1 [46]	10x10x0.1	5	2500	876
IHS	Copper	20x20x1.05	400	8960	390
TIM2	G9 [46]	20x20x0.2	2.87	2500	767
Heat Sink	Copper	60x60x5.5	400	8960	390

2.2. Direct Problem Formulation

Direct problem is solved to simulate thermal tomography temperature measurement data, and it can be formulated by the heat conduction equation for the model shown in Figure 2.4:

$$\nabla[k(\boldsymbol{r})\nabla T(\boldsymbol{r},t)] = C(\boldsymbol{r})\frac{\partial T(\boldsymbol{r},t)}{\partial t}, \tag{2.1}$$

where T is temperature, k is thermal conductivity, C is volumetric heat capacity, and $\boldsymbol{r} = \begin{bmatrix} x & y & z \end{bmatrix}^{\mathrm{T}}$. The initial condition is defined as:

$$T(\boldsymbol{r},0) = T_\infty, \tag{2.2}$$

where T_∞ is the ambient temperature.

The boundary condition equations are given as below where $q''(x,z)$ is heat flux and h_{eff} is the convective heat transfer coefficient to the moving air over the IHS:

$$-k\left(\boldsymbol{r}\right)\left(\frac{\partial T}{\partial y}\right)_{y=0} = q''(x,z)\ ,\ |x| \leq \frac{L_{x,die}}{2}\ ,\ |z| \leq \frac{L_{z,die}}{2}, \tag{2.3}$$

$$\left(\frac{\partial T}{\partial y}\right)_{y=0} = 0\ ,\ |x| > \frac{L_{x,die}}{2}\ ,\ |z| > \frac{L_{z,die}}{2}, \tag{2.4}$$

$$\left(\frac{\partial T}{\partial y}\right)_{y=0} = 0 \ , \ |x| > \frac{L_{x,die}}{2} \ , \ |z| > \frac{L_{z,die}}{2}, \tag{2.5}$$

$$\left(\frac{\partial T}{\partial x}\right)_{x=\pm\frac{L_x}{2}} = 0 \ , \ 0 \leq y \leq L_y \ , \ |z| \leq \frac{L_z}{2}, \tag{2.6}$$

$$\left(\frac{\partial T}{\partial z}\right)_{z=\pm\frac{L_z}{2}} = 0 \ , \ 0 \leq y \leq L_y \ , \ |x| \leq \frac{L_x}{2}, \tag{2.7}$$

$$-k\left(\boldsymbol{r}\right)\left(\frac{\partial T}{\partial y}\right)_{y=L_y} = h_{eff}\left[T\left(\boldsymbol{r},t\right) - T_\infty\right] \ , \ |x| \leq \frac{L_x}{2} \ , \ |z| \leq \frac{L_z}{2}. \tag{2.8}$$

Interface boundary conditions are as follows:

$$-k_i\left(\boldsymbol{r}\right)\left(\frac{\partial T}{\partial x}\right)_{x=L_{x,i^-}} = -k_j\left(\boldsymbol{r}\right)\left(\frac{\partial T}{\partial x}\right)_{x=L_{x,i^+}}, \tag{2.9}$$

$$-k_i\left(\boldsymbol{r}\right)\left(\frac{\partial T}{\partial y}\right)_{y=L_{y,i^-}} = -k_j\left(\boldsymbol{r}\right)\left(\frac{\partial T}{\partial y}\right)_{y=L_{y,i^+}}, \tag{2.10}$$

$$-k_i\left(\boldsymbol{r}\right)\left(\frac{\partial T}{\partial z}\right)_{z=L_{z,i^-}} = -k_j\left(\boldsymbol{r}\right)\left(\frac{\partial T}{\partial z}\right)_{z=L_{z,i^+}}, \tag{2.11}$$

$$T\left(x, y, L_{z,i^-}, t\right) = T\left(x, y, L_{z,i^+}, t\right), \tag{2.12}$$

$$T\left(x, L_{y,i^-}, z, t\right) = T\left(x, L_{y,i^+}, z, t\right), \tag{2.13}$$

$$T\left(L_{x,i^-}, y, z, t\right) = T\left(L_{x,i^+}, y, z, t\right), \tag{2.14}$$

where (i,j) pairs are (die,TIM), (TIM,IHS), (air,IHS) for Equation (2.10), and (air,die), (air,TIM) for Equation (2.9) and Equation (2.11). L_{x,i^-} and L_{x,i^+} denote values approaching $L_{x,i}$ from $+x$ and $-x$ directions, respectively. The same is valid for $L_{y,i}$ and $L_{z,i}$.

Void properties are set equal to those of air in this study. Also, this study defines a void fraction to save computational time by defining k_{TIM} and C_{TIM} in terms of void fractions. The void fraction in a control volume is defined as follows:

$$\varphi = \frac{V_v}{V} \ , \ 0 \leq \varphi \leq 1, \tag{2.15}$$

where φ is the void fraction, and V_v is the volume of the void in a control volume V. There are different alternatives to model the heat capacity and the thermal conductivity of TIM. Volume fraction mixture theory [47] is chosen to calculate TIM's heat capacity and thermal conductivity as follows:

$$C_{TIM} = C_v\varphi + (1-\varphi)\, C_{\text{TIM,ideal}}, \tag{2.16}$$

$$k_{TIM} = k_v\varphi + (1-\varphi)\, k_{\text{TIM,ideal}}, \tag{2.17}$$

where k_v and C_v are the thermal conductivity and the heat capacity of void, respectively.

The temperature distribution of the system can be found for a given void fraction distribution since the governing equation, initial condition, boundary equations, and material properties are all known in the direct heat conduction problem. Different numerical solution methods can be used to solve the direct problem [48].

In this study, the system shown in Figure 2.3 is modeled and solved using commercial finite volume software ANSYS Icepak due to its ease of use, whereas the system shown in Figure 2.4 is modeled using a developed MATLAB code. In the code, the rectangular domain with dimensions $L_x \times L_y \times L_z$ is divided into $N = N_x \times N_y \times N_z$ sub elements with $(N_x + 1) \times (N_y + 1) \times (N_z + 1)$ volumes. Die, TIM, IHS, and air's thermal conductivity and heat capacity are assigned to these volumes according to their location. Then, the finite volume method is used with implicit formulation to solve the transient heat transfer problem. The equations of the finite volume method are equivalent to the equations of the finite difference method in this problem. The MATLAB code developed is used to solve the direct problem for the thermal tomography test as thermophysical properties to each volume can be assigned in the code. Besides, it can reach solutions faster than commercial finite element software such as COMSOL Multiphysics. This feature is essential considering that the direct problem is solved repeatedly during the inverse problem solution through iterations.

2.3. Verification of Direct Problem Solution

A verification study for modeling the heat capacity and the thermal conductivity of TIM is carried out to validate the accuracy of the volume fraction mixture theory [47]. First, an actual void with 0.1 mm^3 volume is added to the center of the TIM, and the direct problem explained in Section 2.2 is modeled and solved using ANSYS Icepak. Then, a 0.33 void fraction is assigned to a volume of 0.3 mm^3 at the center of the TIM. The heat capacity and the thermal conductivity of TIM are calculated using Equations (2.16) and (2.17), and the direct problem explained in Section 2.2 is modeled and solved using ANSYS Icepak. Temperature variation over the IHS is obtained for both cases, and their difference is shown in Figure 2.5. The maximum difference is 0.058 °C, indicating that predictions of the volume fraction mixture theory show good agreement with the actual void case.

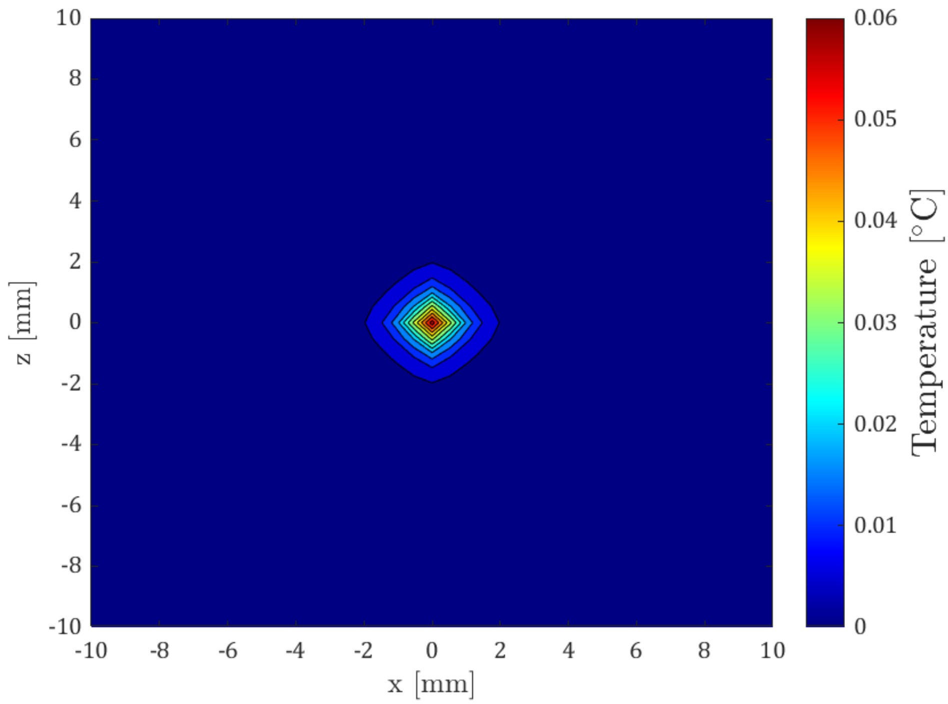

Figure 2.5. Difference of temperature distributions over the IHS between the volume fraction mixture theory and the actual void cases (t=100 ms).

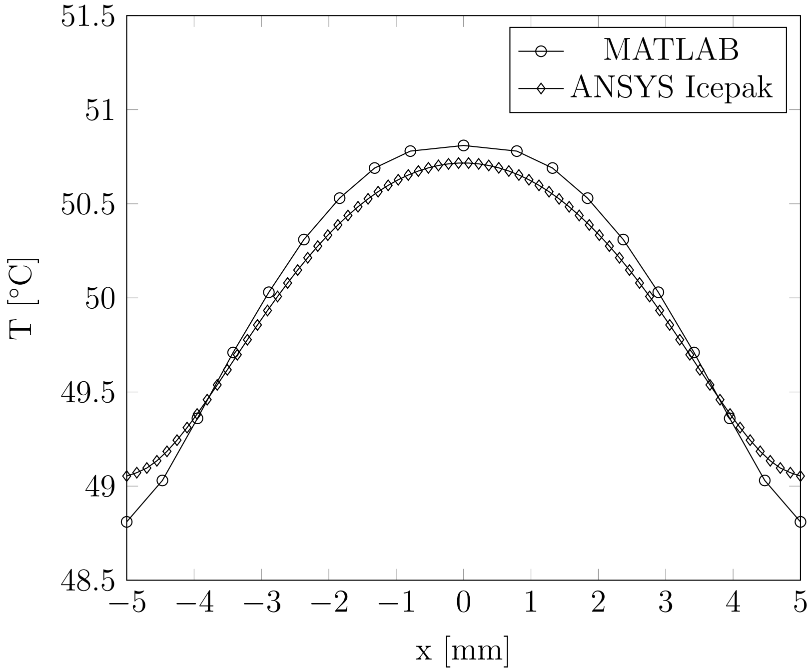

Figure 2.6. Temperature variation comparison at the bottom surface of the die at t=100 ms along the x-axis (y=0, z=0) for MATLAB and ANSYS Icepak.

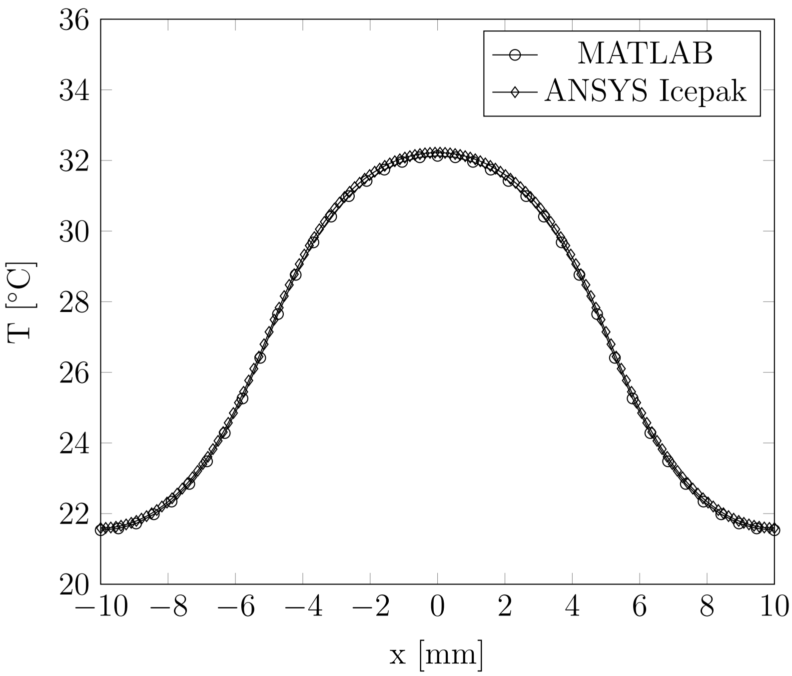

Figure 2.7. Temperature variation comparison over the IHS at t=100 ms along the x-axis (y=1.7 mm, z=0) for MATLAB and ANSYS Icepak.

A verification study for the MATLAB code developed is also carried out to validate the accuracy of the direct problem solution. The direct problem explained in Section 2.2 is modeled and solved using a commercial software ANSYS Icepak to compare the results obtained by MATLAB code. Temperature variations at the bottom surface of the die for both MATLAB and ANSYS Icepak solvers are shown in Figure 2.6. Maximum die temperatures for MATLAB and Icepak are found as 50.8 °C and 50.7 °C, respectively. Temperature variation over the IHS for MATLAB and ANSYS Icepak solvers is also shown in Figure 2.7. Predictions of the MATLAB code show good agreement with the ANSYS Icepak results and underline the verification of the MATLAB model.

2.4. Inverse Problem Formulation

The simulated temperature measurements are obtained from the upper surface of IHS by solving the direct problem mentioned above. Then, a total of $M = M_x \times M_y$ temperature measurement points can be uniformly selected. These temperature measurement points are defined as:

$$T^{mea}_{m,s} = \begin{bmatrix} T^{mea}_{1,1} & T^{mea}_{1,2} & \dots & T^{mea}_{1,S} \\ T^{mea}_{2,1} & T^{mea}_{2,2} & \dots & T^{mea}_{2,S} \\ \vdots & \vdots & \ddots & \vdots \\ T^{mea}_{M,1} & \alpha_{M,2} & \dots & T^{mea}_{M,S} \end{bmatrix}, \tag{2.18}$$

where s and S represent different measurement times and total number of measurement times, respectively. All measurements are subject to random measurement error due to the instrument's measurement uncertainty; an error with a normal distribution is introduced to the solution of the direct problem for establishing $T^{mea}_{m,s}$.

Similarly, a total of $G = G_x \times G_y \times G_z$ uniformly distributed sub volumes are considered in TIM. These sub volumes are where void fractions have represented. The IHS upper surface temperature field can be determined, represented as $T^{cal}_{m,s}(\varphi^n_g)$ for a given void fraction vector $\varphi_g^n = [\varphi_1^n,\ \ \varphi_2^n,\ \ \cdots\ \ ,\ \varphi_G^n]^{\mathrm{T}}$ and thermal boundary conditions by solving the direct problem again.

The inverse problem is the estimation of void fractions by iterations using the M measured temperature points for S measurement times to minimize the objective function defined as follows:

$$J(\varphi_g^n) = \sum_{m=1}^{M} \sum_{s=1}^{S} \left(T_{m,s}^{cal}(\varphi_g^n) - T_{m,s}^{mea} \right)^2 . \tag{2.19}$$

3. METHODOLOGY

3.1. Fuzzy Inference Method

The inverse property estimation for identifying the void fraction distribution in TIM by the fuzzy inference method is shown in Figure 3.1 as a block diagram. The system includes a set of one-dimensional fuzzy inference units ($\mathrm{FIU_m}$) which carry out the fuzzy inference process to generate the fuzzy inference results Δu_m by using the temperature deviation $e_m(\varphi_g^n) = [e_1, \quad e_2, \quad \cdots \quad , \ e_M]^{\mathrm{T}}$ at each mth measurement point. The equation for the temperature deviation calculation is given below:

$$e_{m,s}(\varphi_g^n) = T_{m,s}^{cal}(\varphi_g^n) - T_{m,s}^{mea}, \tag{3.1}$$

$$e_m(\varphi_g^n) = \frac{1}{S}\sum_{s=1}^{S} e_{m,s}, \tag{3.2}$$

where $T_{m,s}^{cal}(\varphi_g^n)$ and $T_{m,s}^{mea}$ represent the calculated and measured temperature at the mth measurement point for sth measurement time, respectively.

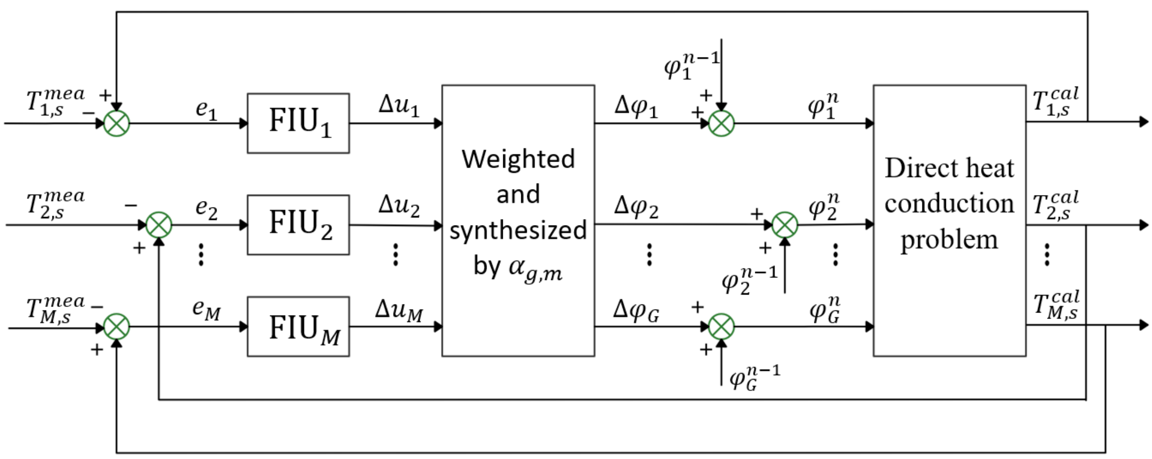

Figure 3.1. Block diagram for the decentralized fuzzy inference system (Adapted from [44]).

First, the fuzzification process is performed in the FIM. The domains of the input variable e_m and the output variable Δu_m for the decentralized $\mathrm{FIU_m}$ are set as $[-p_e, \ \ p_e]$ and $[-p_u, \ \ p_u]$, respectively. Seven fuzzy sets are separately defined for input variable e_m and output variable Δu_m. These fuzzy sets are labeled in the same linguistic terms of negative big (NB), negative medium (NM), negative small (NS), zero (ZO), positive small (PS), positive medium (PM), and positive big (PB). The membership degrees of these fuzzy sets can be determined using the triangle functions which are shown in Figure 3.2 [39].

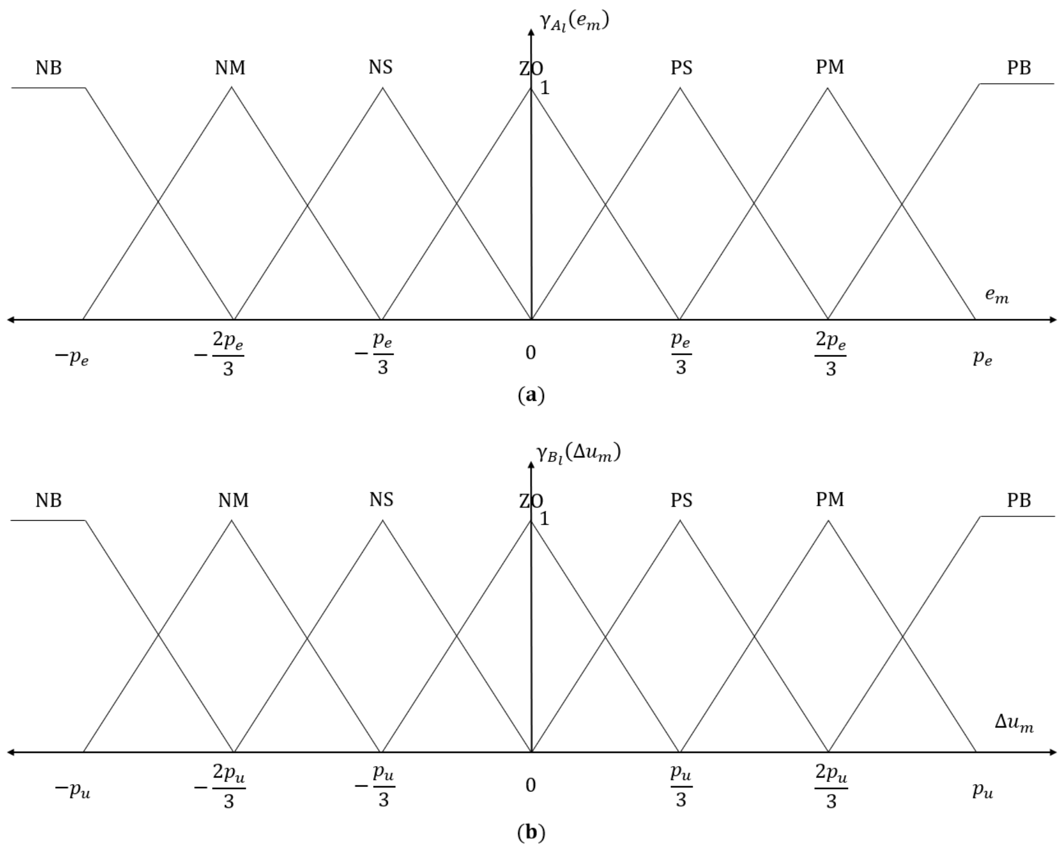

Figure 3.2. Membership functions of (a) e_m and (b) Δu_m for fuzzy sets.

As a next step, fuzzy inference rules are identified and performed. The rules are chosen according to the qualitative knowledge of the heat conduction process. When only considering error at the mth measurement point, if $e_m > 0$, it means that the calculated temperature at the mth measurement point, T_m^{cal}, is higher than the measured temperature, T_m^{cal}. In this case, the guessed void fraction should be increased to minimize the error, e_m; in other words, the fuzzy inference should result in $\Delta u_m > 0$. Also, for bigger values of e_m, the guessed void fraction must be increased more accordingly, or vice versa. The fuzzy inference rules of $\mathrm{FIU_m}$ for this study are listed in Table 3.1.

Table 3.1. Fuzzy inference rules.

e_m	NB	NM	NS	ZO	PS	PM	PB
Δu_m	NB	NM	NS	ZO	PS	PM	PB

The most commonly used fuzzy inference method, the Max-Min inference engine, or Mamdani inference engine [49] is used to calculate the fuzzy set B of Δu_m^* at the domain $[-p_u, \quad p_u]$:

$$\gamma_B\left(\Delta u_m^*\right) = \max_{l=1}^{7}\left\{\min\left[\gamma_{A_l}\left(e_m\right), \gamma_{B_l}\left(\Delta u_m^*\right)\right]\right\}, \tag{3.3}$$

where $\gamma_{A_l}(e_m)$ and $\gamma_{B_l}(\Delta u_m^*)$ are the membership degree of e_m and Δu_m, respectively.

Finally, defuzzification procedure is employed to obtain each Δu_m. The fuzzy inference result Δu_m for the corresponding temperature deviation e_m is obtained by the center of gravity method [50] as follows:

$$\Delta u_m = \frac{\displaystyle\int_{-p_u}^{p_u} \gamma_B\left(\Delta u_m^*\right) \Delta u_m^* \mathrm{d}\Delta u_m^*}{\displaystyle\int_{-p_u}^{p_u} \gamma_B\left(\Delta u_m^*\right) \mathrm{d}\Delta u_m^*}, \tag{3.4}$$

where each Δu_m is calculated by Fuzzy Logic Toolbox in MATLAB.

The inference result Δu_m of $\mathrm{FIU_m}$ is the compensation for the guessed void fraction of all sub volumes when only the mth measured temperature is considered. In reality, the void fraction at all sub volumes affects the temperature at more than one measurement points. Thus, the temperature at all measurement points should be considered synthetically to adjust the guessed void fraction at all sub volumes. The adjustments to the void fraction profile at all sub volumes can be calculated as follows:

$$\begin{bmatrix} \Delta\varphi_1 \\ \Delta\varphi_2 \\ \vdots \\ \Delta\varphi_G \end{bmatrix} = \begin{bmatrix} \alpha_{1,1} & \alpha_{1,2} & \dots & \alpha_{1,M} \\ \alpha_{2,1} & \alpha_{2,2} & \dots & \alpha_{2,M} \\ \vdots & \vdots & \ddots & \vdots \\ \alpha_{G,1} & \alpha_{G,2} & \dots & \alpha_{G,M} \end{bmatrix} \begin{bmatrix} \Delta u_1 \\ \Delta u_2 \\ \vdots \\ \Delta u_M \end{bmatrix}, \tag{3.5}$$

where $\alpha_{g,m}$ is the weighting coefficient, and its sum must be equal to 1.

The weighting coefficient $\alpha_{g,m}$ denotes the impact of φ_g at the gth sub volume on the temperature at the mth measurement point. This study follows a weighted approach with the three-dimensional normal distribution that specifies the weighting coefficient $\alpha_{g,m}$ as follows:

$$\alpha_{g,m} = \frac{\exp\left\{-\left[(x_g - x_m)^2/\theta_1^2 + (y_g - y_m)^2/\theta_2^2 + (z_g - z_m)^2/\theta_3^2\right]\right\}}{\sum\limits_{m=1}^{M} \exp\left\{-\left[(x_g - x_m)^2/\theta_1^2 + (y_g - y_m)^2/\theta_2^2 + (z_g - z_m)^2/\theta_3^2\right]\right\}}, \tag{3.6}$$

where $(g = 1, 2, \dots, G)$, $(m = 1, 2, \dots, M)$, x, y, z are the coordinates of sub volumes and measurement points, and $\theta_1, \theta_2, \theta_3 > 0$ are the variation coefficients of the three-dimensional normal distribution.

After weighting and synthesizing the fuzzy inference results, the guessed void fraction distribution is updated as following:

$$\varphi_g^n = \varphi_g^{n-1} + \Delta\varphi_g \quad (g = 1, 2, \cdots, G), \tag{3.7}$$

where n denotes for the number of iterations.

The stopping criterion applied in the inverse estimation process is shown as follows:

$$J(\varphi_g^n) = \sum_{m=1}^{M} \sum_{s=1}^{S} \left(T_{m,s}^{cal}(\varphi_g^n) - T_{m,s}^{mea}\right)^2 \leq \mathcal{E}, \tag{3.8}$$

where convergence criteria $\mathcal{E}$ is a specified small positive number. The convergence criteria is chosen as $\mathcal{E}$=0.01 °C^2 for problems using simulated data with no random error, and $\mathcal{E} = M \times S \times \sigma^2$ for problems using simulated data with random error introduced based on a standard deviation σ. The solution algorithm for FIM is presented in Figure 3.3.

(i) Initial guess: φ_g^0, n=1

(ii) $T_{m,s}^{cal}(\varphi_g^0)$ from Equations (2.1)-(2.17)

(iii) $J(\varphi_g^0)$ from Equation (2.19)

(iv) While $(J(\varphi_g^{n-1}) > \mathcal{E})$

- (a) Δu_m from Equations (3.1)-(3.4)
- (b) $\alpha_{g,m}$ from Equation (3.6)
- (c) $\Delta\varphi_g$ from Equation (3.5)
- (d) φ_g^n from Equation (3.7)
- (e) $T_{m,s}^{cal}(\varphi_g^n)$ from Equations (2.1)-(2.17)
- (f) $J(\varphi_g^n)$ from Equation (2.19)
- (g) $n = n + 1$

Figure 3.3. Fuzzy Inference Method.

4. RESULTS AND DISCUSSIONS

4.1. Grid Independence Study

All numerical simulations are subject to discretization error due to the use of a finite number of grid points. It is essential to verify that the solution of a numerical problem is insensitive to the grid resolution; therefore, a grid refinement study should be carried out [51]. For this purpose, simulations with different mesh sizes are performed and compared for Test-1 and Test-2. The Grid Convergence Index (GCI), which is one of the most common grid refinement methods proposed by Roache [52], is used to verify the grid independence of numerical models.

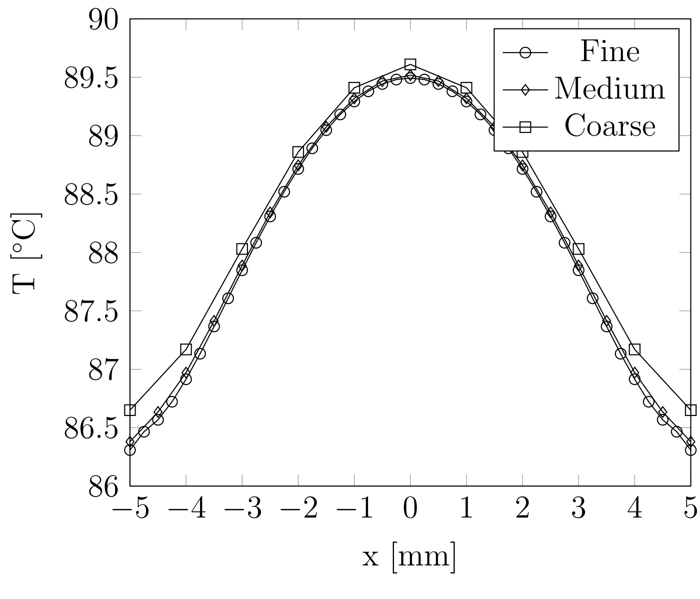

Figure 4.1. The results of grid refinement study on temperature variation at the bottom surface of the die along the x-axis (y=0, z=0) for Test-1.

In Test-1, the problem is modeled and solved using ANSYS Icepak. The grid refinement study is performed for coarse, medium, and fine meshes using the hex-dominant mesher consisting mainly of hexahedral elements. The details for three mesh types are given in Table 4.1, along with the maximum die temperatures T_j for all cases.

Table 4.1. Mesh details of Icepak model for Test-1.

Grid Type	**Maximum Element Size [mm]**	**Total Node Number**	T_j **[°C]**
Fine	0.25	4588399	89.49
Medium	0.5	1156639	89.52
Coarse	1	293959	89.60

Temperature variation at the bottom surface of the die for all cases is presented in Figure 4.1 to compare the results of different mesh types in Test-1. All three cases exhibit the same trend in terms of temperature variation, and the results show a tendency to converge as the mesh type goes from medium to fine. The junction temperatures, T_j, and the total number of nodes given in Table 4.1 are used to calculate GCI values. For fine and medium grids, GCI_{12} is calculated as 0.025, while for medium and coarse grids, GCI_{23} is found as 0.067. Therefore, the grids are in the asymptotic range of convergence, and the Icepak model solved in Test-1 is considered grid independent.

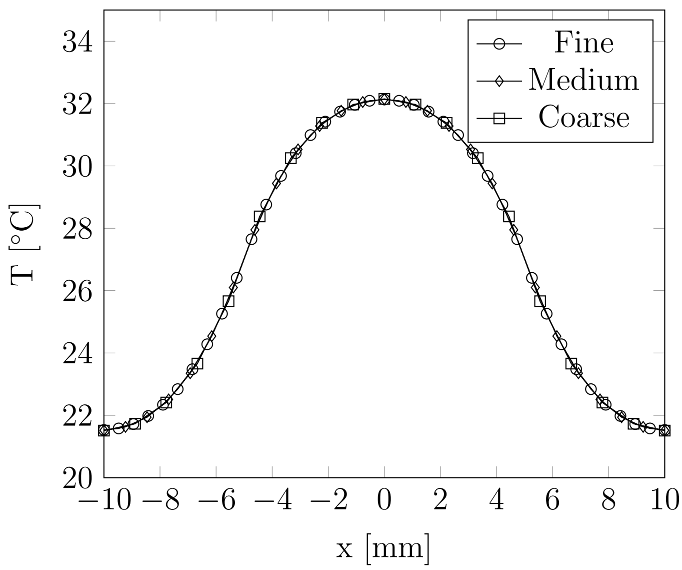

Figure 4.2. The results of grid refinement study on temperature variation over the IHS at t=100 ms along the x-axis (y=1.7 mm, z=0) for Test-2.

In Test-2, the problem is modeled and solved using the developed MATLAB code. The grid refinement study is performed for coarse, medium, and fine meshes using a rectangular prism shaped elements with $(N_x + 1) \times (N_y + 1) \times (N_z + 1)$ nodes. The details for three mesh types are given in Table 4.2, along with the maximum die temperatures T_j for all cases.

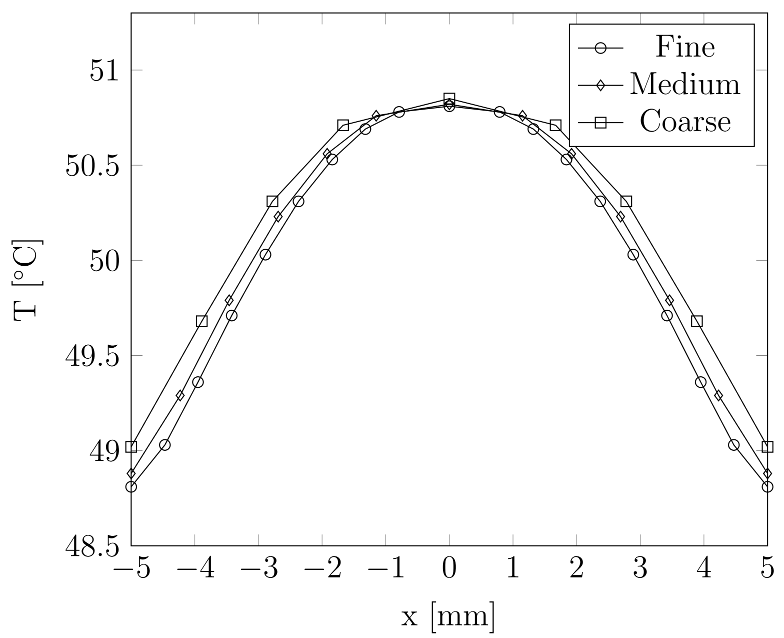

Figure 4.3. The results of grid refinement study on temperature variation at the bottom surface of the die at t=100 ms along the x-axis (y=0, z=0) for Test-2.

Temperature variation over the IHS and at the die bottom surface for Test-2 are presented in Figure 4.2 and 4.3, respectively. In Figure 4.2, the temperature distribution is identical for all mesh types, and Figure 4.3 illustrates that the temperature distributions of different meshes show the same trend. Also, GCI_{12} is calculated as 0.012 for fine and medium grids, while GCI_{23} is found as 0.037 for medium and coarse grids using the junction temperatures and the total number of nodes given in Table 4.2. As a result, the grids are found in the asymptotic range of convergence, and the developed MATLAB model solved in Test-2 is regarded as grid independent. In this research, fine meshes are employed for both tests.

Table 4.2. Mesh details of the developed MATLAB model for Test-2.

Grid Type	**Maximum Element Size [mm]**	**Total Node Number**	T_j **[°C]**
Fine	0.53	27378	50.81
Medium	0.77	13122	50.82
Coarse	1.11	6498	50.85

4.2. Temperature Measurement Simulations

The temperature measurement data, which is supposed to be evaluated by actual testing devices, is simulated by solving the direct heat transfer problem for a given void fraction in this research. First, the effect of voids in the thermal performance test (Test-1) is investigated to see whether the voids have an apparent impact on the temperature distribution of the package.

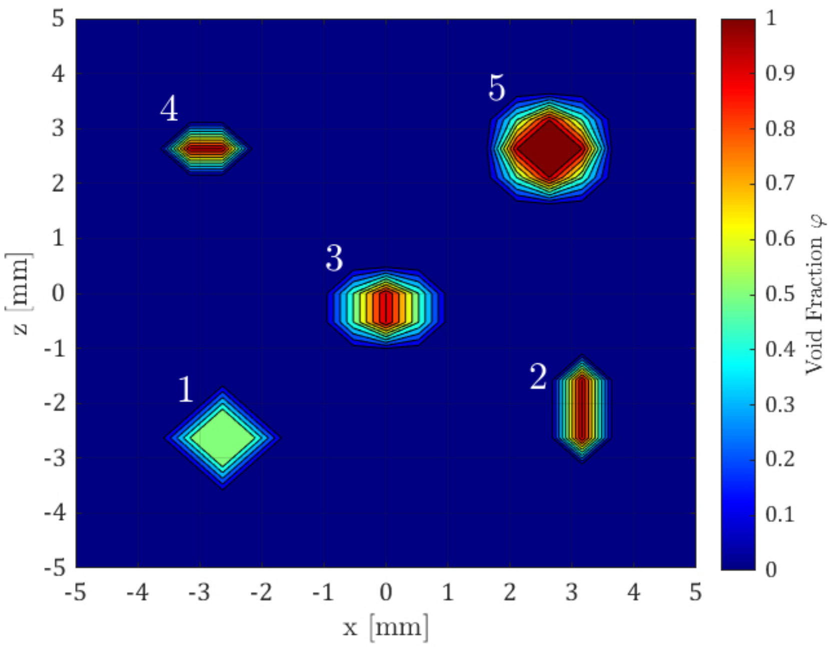

Figure 4.4. Actual void fraction distribution across TIM1.

Table 4.3. Individual effects of voids on thermal performance test (Test-1).

	Void 1	**Void 2**	**Void 3**	**Void 4**	**Void 5**
ΔT_j [°C]	0.1	0.2	1.7	0	1
ΔT_{local} [°C]	1.1	2.7	1.7	1.9	3.3

Void fraction distribution across TIM1, which is to be identified by the thermal tomography test (Test-2), is illustrated in Figure 4.4. The effects of five voids on the temperature increase in Test-1 are investigated one at a time before examining their combined effect together. Table 4.3 shows how much the maximum die temperature and the temperature at the void location increase for each void. Relatively small voids such as Void 1 and Void 4 cause a smaller temperature increase than the larger ones like Void 5. It can be seen that the locations of voids also play a significant role in junction temperature increase. For instance, Void 2 creates a considerable local temperature increase at its center; however, it does not make a noticeable difference in the junction temperature. The voids that do not considerably increase the junction temperature show that their effects on the thermal performance test are less significant than the others. However, identifying these voids is substantial in terms of discovering the limits of the proposed method.

Thermal performance test (Test-1) is conducted by following the procedure explained in Section 2.1. The simplified model illustrated in Figure 2.3 is solved using ANSYS Icepak with voids shown in Figure 4.4 and without voids. The comparison of these two cases is shown in Figure 4.5 by means of temperature distribution at the die bottom surface. Figure 4.5 indicates that the maximum die temperature increases by 2.1 °C for the case with voids.

Considering the voids have a measurable impact on the temperature distribution of the die during the thermal performance test, the identification of void locations and sizes is required through the thermal tomography test (Test-2). Thermal tomography test follows the procedure explained in Sections 2.1 and 2.2. The simplified model illustrated in Figure 2.4 is solved with assigned void fractions given in Figure 4.4 using the developed MATLAB code. The temperature distribution over the IHS is recorded with 10 ms intervals during the solution of the direct problem. These recordings, also referred to as simulated measurements, are used in place of experimental data for evaluating the proposed method, which is supposed to be captured by an IR camera.

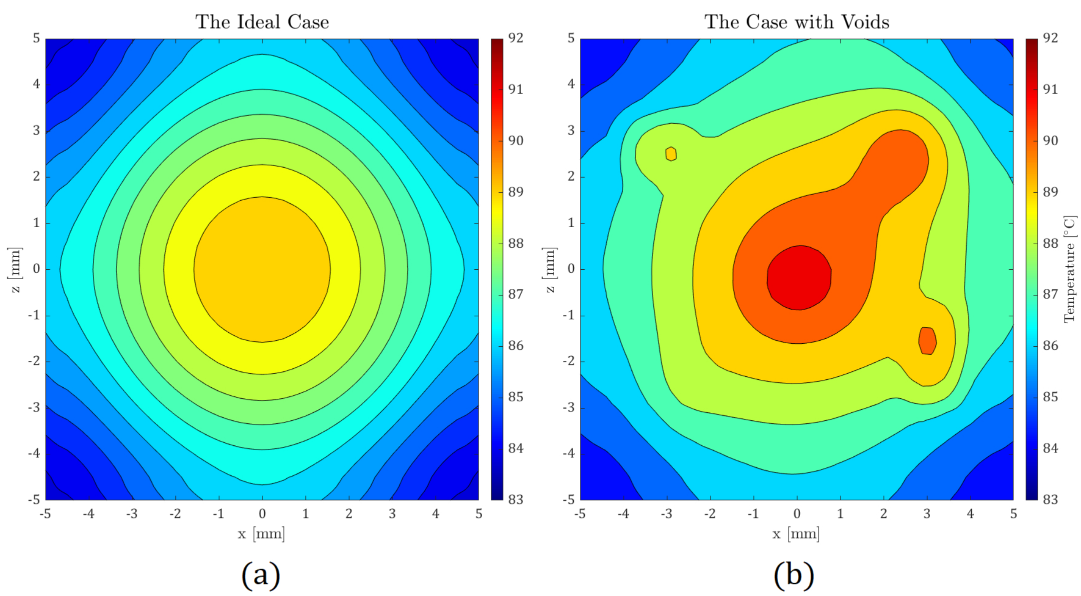

Figure 4.5. Temperature distribution of the die bottom surface (y=0) in Test-1 (a) without voids and (b) with five voids.

Figure 4.6 illustrates simulated temperature measurements with 10 ms intervals. All measurements are subject to random measurement error due to instrument's measurement uncertainty, which makes it very challenging to solve inverse problems due to their instable nature. Scientific cameras with photon-based and cryogenically cooled detectors have a measurement uncertainty of $\sigma = 0.02$ °C, with 95% of the random error lying within $\pm 2\sigma$ [53]. A random measurement error based on a Gaussian distribution with a standard deviation of $\sigma = 0.02$ °C is introduced to simulated measurements to produce the synthetic measurement data. Synthetic measurement data is illustrated in Figure 4.7, with 99.7% of the introduced random error lying within $\pm 3\sigma$.

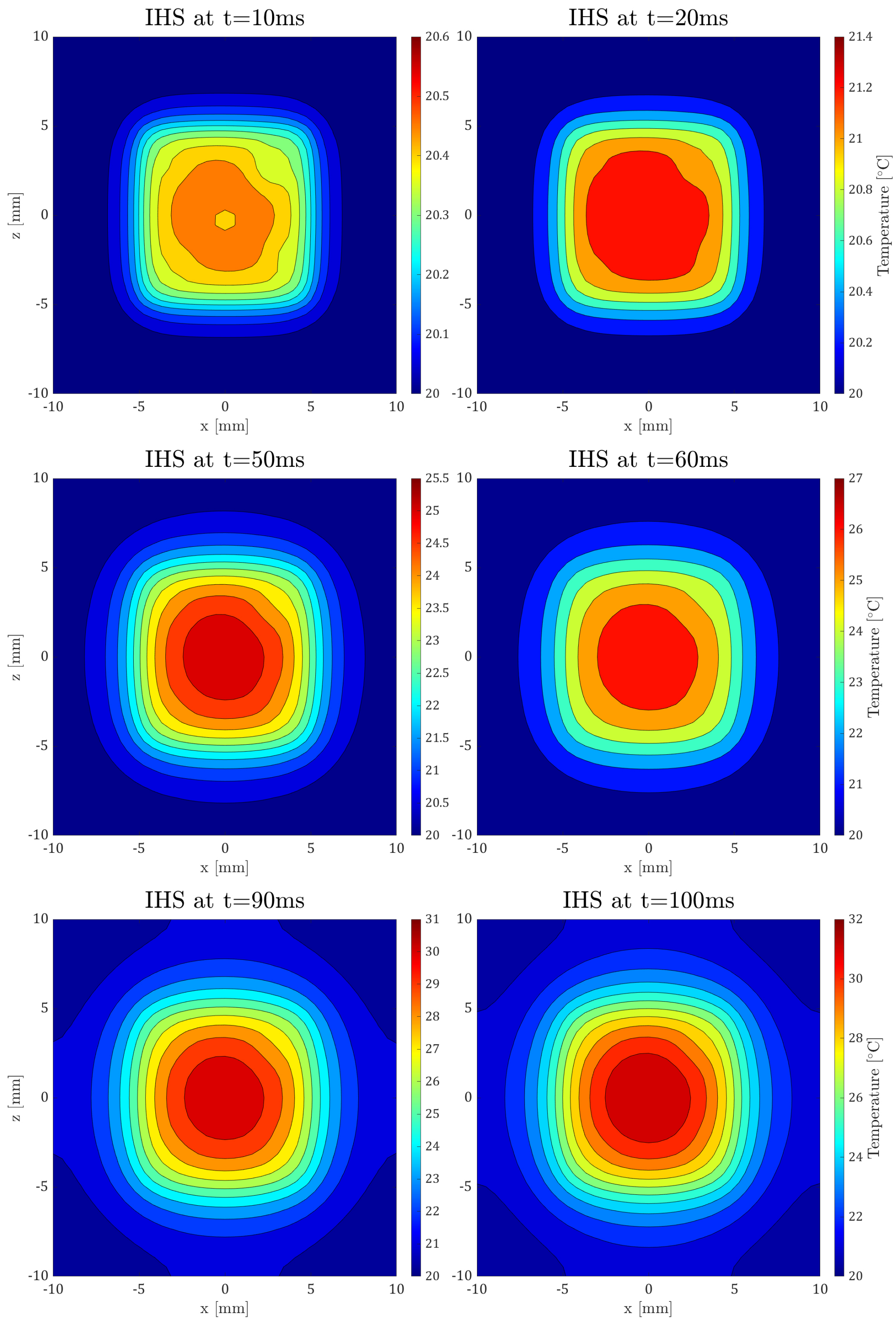

Figure 4.6. Simulated measurements of IHS temperature distribution for the case including voids without introducing measurement errors.

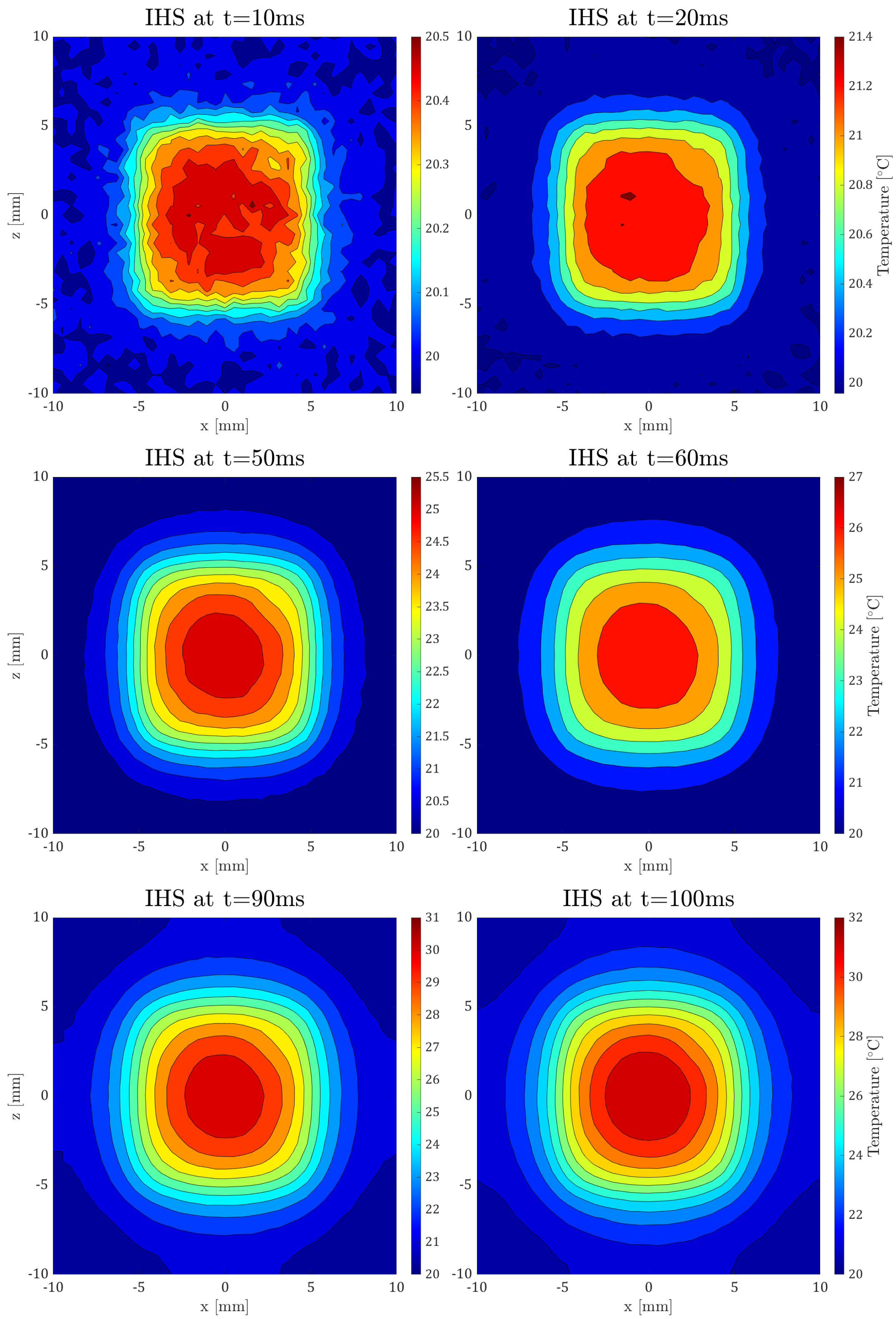

Figure 4.7. Synthetic measurement data obtained by introducing random error to simulated measurements ($\sigma = 0.02$ °C).

4.3. Void Fraction Estimation

Temperature measurements illustrated in Figures 4.6 and 4.7 are used to quantitatively characterize voids in TIM by estimating the void fractions using the fuzzy inference method. A constant uniform die power of 90 W is applied for 100 ms to heat the package. The power map is a constant uniform heat flux $q''(x, z)$ of 90 W/cm^2 applied to the bottom surface of the die as a step function that starts at t=0 ms. Although power maps used in real-life applications usually have non-uniform and temporal distribution, a simplified power map function is considered in this study. The period and duration of measurements (t=10 ms to 100 ms) are chosen to portray system reaction while preserving the die from overheating. During the thermal tomography test, the maximum die temperature reaches 53.5 °C, far below the temperatures that the die gets harmed.

First, the case of simulated measurements without measurement error, as shown in Figure 4.6, is considered to estimate void fractions within TIM. The solution of this case is referred to as "inverse crime" as the same model is used for mapping between the synthetic measurements and its inversion. However, this is a required setup for testing the method's reliability before moving on to the more realistic or demanding example with measurement data containing errors, as shown in Figure 4.7.

A total of $39 \times 39 = 1521$ uniformly distributed temperature measurement points, $T^{mea}_{m,s}$, are selected over the IHS according to the grid independence study explained in Section 4.1. Similarly, a total of $19 \times 19 = 361$ uniformly distributed sub volumes, φ^n_g, are considered in TIM layer. As an initial guess, TIM is considered to be ideal, which means that there is no void within TIM (φ^0_g=0). The domains of the input variable e_m and the output variable Δu_m for the decentralized $\mathrm{FIU_m}$ are set as $p_e = 1$ °C and $p_u = 0.2$, respectively. The three-dimensional normal distribution weighting coefficient matrix, $\alpha_{g,m}$, is calculated with $\theta_1 = \theta_2 = \theta_3 = 0.075$ variation coefficients. The convergence criteria, $\mathcal{E}$, is defined as 0.01 for the case of without measurement error as suggested in [2, 44, 45].

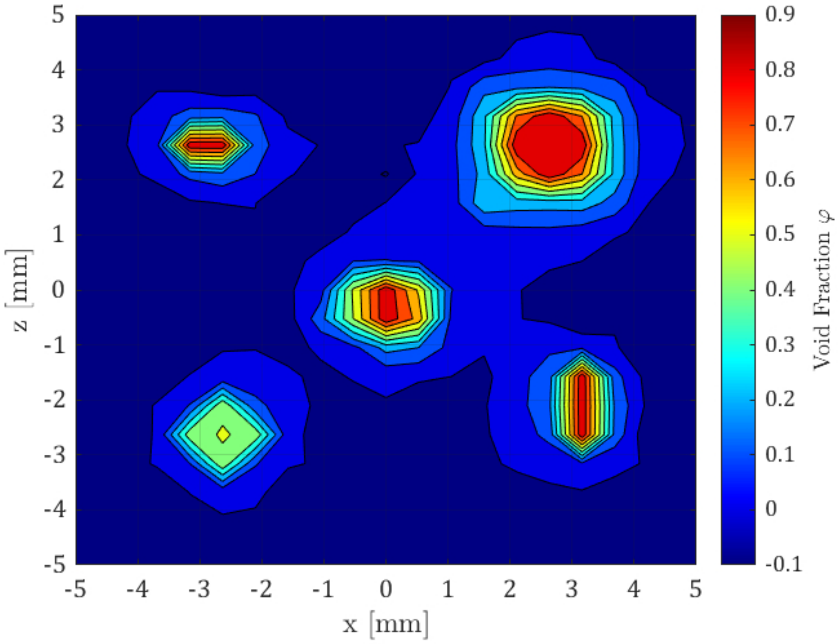

Figure 4.8. Estimated void fractions in TIM without any measurement error ($\sigma = 0$ °C).

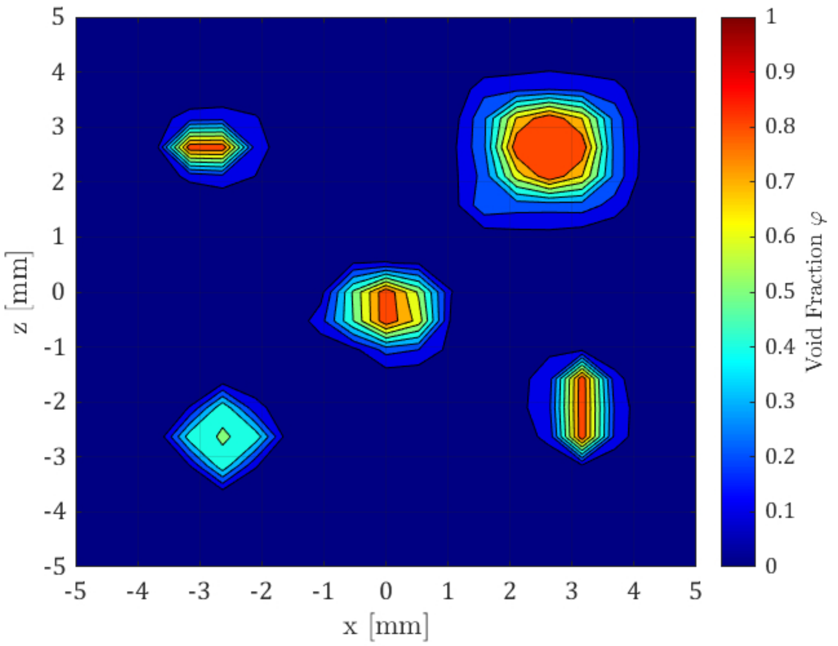

Figure 4.9. Ad-hoc filtered estimated void fractions in TIM without any measurement error ($\sigma = 0$ °C).

Figure 4.8 illustrates estimated void fractions in TIM for the case of simulated measurements without measurement error. Calculated results are out of the physically possible range [0,1] for some of the sub volumes. Therefore, ad-hoc filtering is applied to eliminate this problem by equating values greater than 1 to 1 and values less than 0 to 0. The results are illustrated in Figure 4.9. The average absolute error after the ad-hoc filtering is 0.033, whereas the maximum absolute error is 0.28 for the case shown in Figure 4.9. Each iteration uses about 20 seconds with Intel® i5 processor with 1.80 GHz frequency, and the convergence is achieved after 50 iterations.

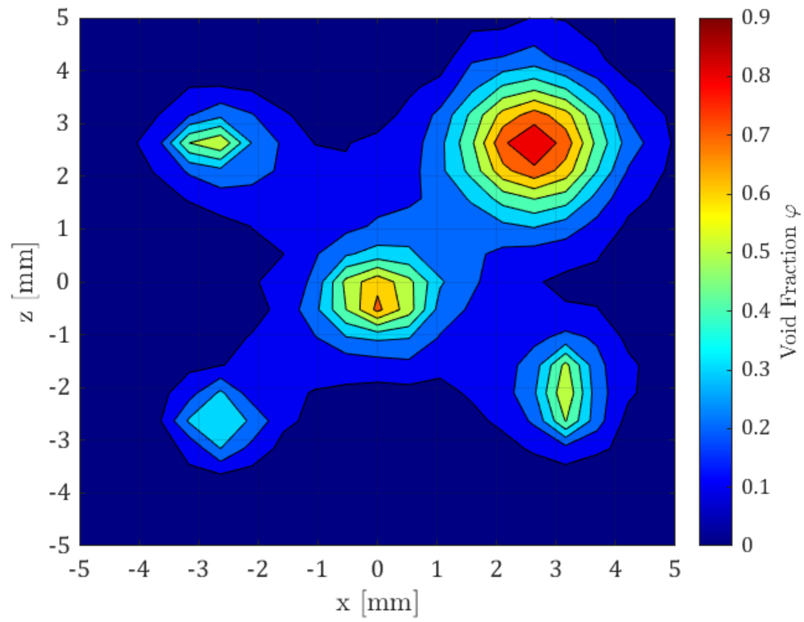

Figure 4.10. Ad-hoc filtered estimated void fractions in TIM with normally distributed random measurement error with $\sigma = 0.02$ °C.

The same procedure is performed for the synthetic measurement data with a normally distributed random measurement error with $\sigma = 0.02$ °C. Here, the convergence criteria, $\mathcal{E}$, is calculated according to the discrepancy principle [31] as $\mathcal{E} = M \times S \times \sigma^2$ where M, S, and σ represent the number of temperature measurement points, the number of temperature measurement times, and the standard deviation of the random measurement error introduced, respectively. Figure 4.10 illustrates the ad-hoc filtered estimated void fractions in TIM for the case of synthetic measurement data with a normally distributed measurement error of $\sigma = 0.02$ °C. Convergence is achieved in less than 30 iterations due to the significant increase in the convergence criteria. In the meantime, the void fractions are estimated less accurately compared to the case with no measurement errors. The average absolute error is 0.11, whereas the maximum absolute error is 0.50 for the case shown in Figure 4.10.

Void fraction estimations for synthetic measurement data with normally distributed random measurement errors with 2σ and 3σ are also illustrated in Figure 4.11 and Figure 4.12, respectively. The average absolute errors are 0.14 and 0.19, whereas the maximum absolute errors are 0.55 and 0.67 for the cases with 2σ and 3σ measurement errors, respectively. Convergence is achieved in less than 20 iterations due to a considerable increase in the convergence criteria for the synthetic measurement data with 2σ and 3σ errors. However, the prediction accuracy decreases even more than the case with normally distributed error of $\sigma = 0.02$ °C. Also, the voided regions appear to expand and connect the areas between the actual void locations in all cases except the "inverse crime" one.

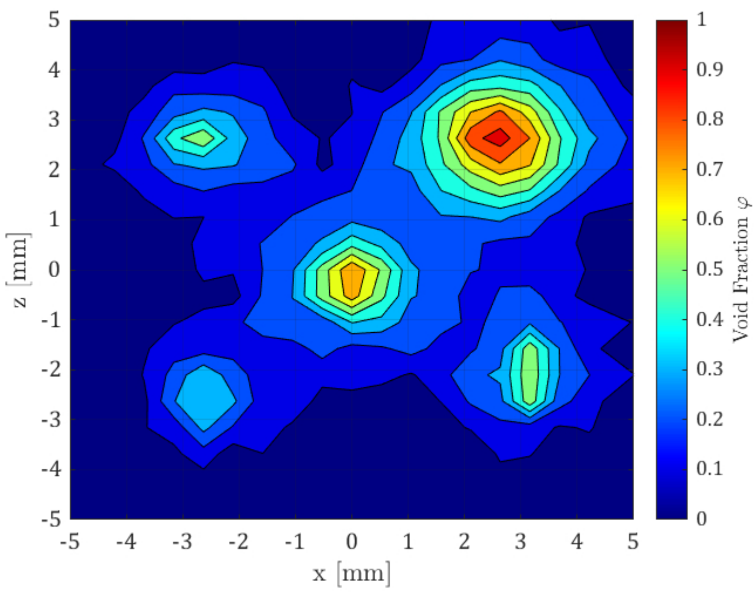

Figure 4.11. Ad-hoc filtered estimated void fractions in TIM with normally distributed random measurement error with $\sigma = 0.04$ °C.

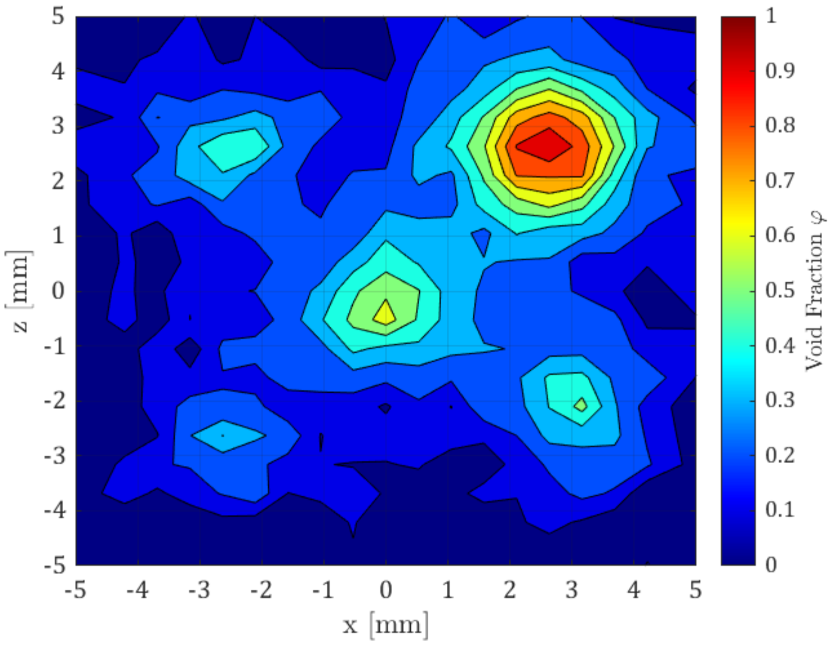

Figure 4.12. Ad-hoc filtered estimated void fractions in TIM with normally distributed random measurement error with $\sigma = 0.06$ °C.

Effects of different test parameters should be determined to see the proposed method's limits. First, effect of applied die power is investigated. The effect of die power used for the test for void fraction estimation is compared using 80 W, 90 W, and 100 W die power with 100 ms test duration. The results are illustrated in Figure 4.13. The average absolute errors are 0.13, 0.14, and 0.14, whereas the maximum absolute errors are 0.60, 0.55, and 0.55 for the cases using 80 W, 90 W, and 100 W die power, respectively. The void fraction estimations appear similar in Figure 4.13, and the average absolute errors are almost identical. Maximum absolute error results show that the prediction accuracy slightly improves when the die power used for the test is increased from 80 W to 90 W. However, there is almost no change in void fraction prediction accuracy when the die power used is increased from 90 W to 100 W. Further increase in applied die power is expected to improve the estimation accuracy, but it would restrict the test duration as the die reaches maximum operating temperature faster. As a result, 90 W die power is selected to be used in the test.

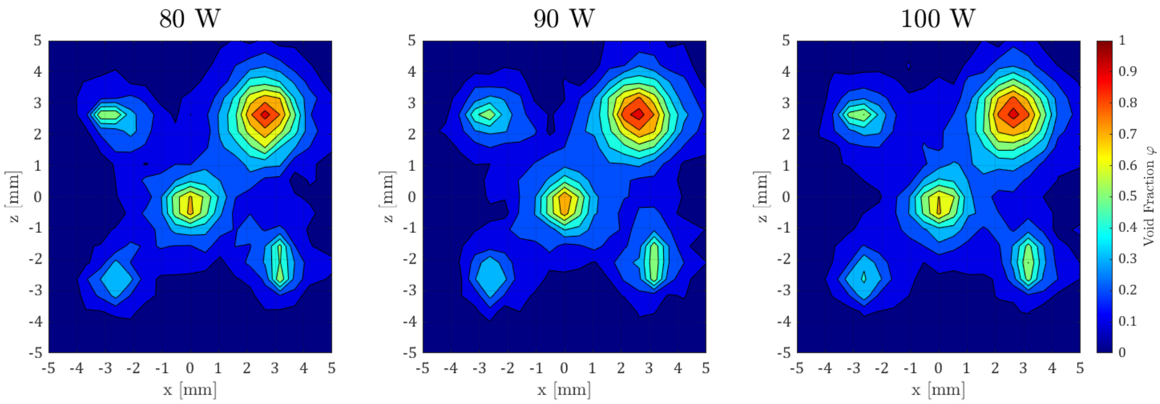

Figure 4.13. Ad-hoc filtered estimated void fractions in TIM when different die powers are applied ($\sigma = 0.04$ °C).

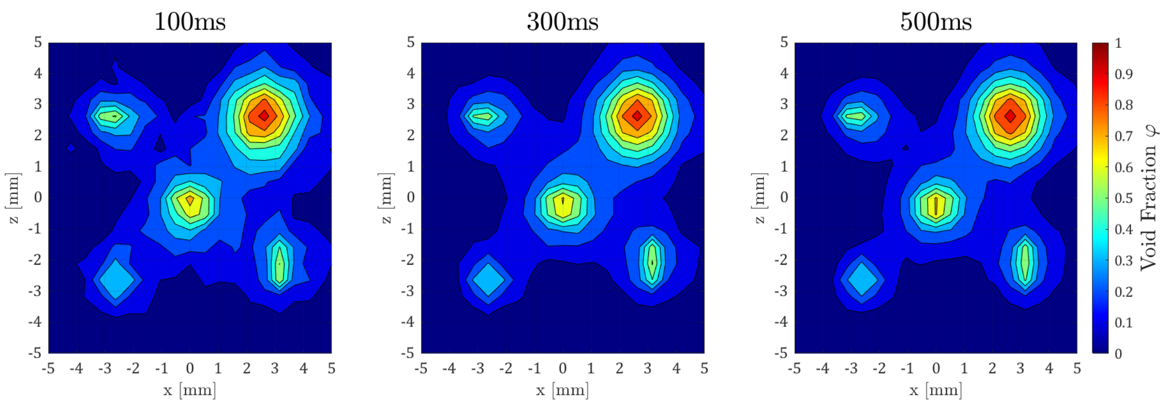

Figure 4.14. Ad-hoc filtered estimated void fractions in TIM for different test duration ($\sigma = 0.04$ °C).

Similarly, effect of test duration is investigated to see the limits of the proposed method. The effect of test duration on void fraction estimation is compared using 100 ms, 300 ms, and 500 ms test duration with 10 ms intervals. The results are shown in Figure 4.14. The average absolute errors are 0.14, 0.12, and 0.12, whereas the maximum absolute errors are 0.52, 0.53, and 0.54 for the cases with 100 ms, 300 ms, and 500 ms test duration, respectively. During the 500 ms test, the maximum die temperature reached 83 °C, below the maximum operating temperature. Figure 4.14 shows that the extension of test duration from 100 ms to 300 ms leads to more accurate prediction results. The void fractions around and between the actual voids are observed to decrease, and the geometry and the size of voids become more distinguishable. More temperature measurement data is obtained with the prolongation of the test period, which helps to reduce the noise due to random temperature measurement error by increasing sample size. However, the increase in temperature measurement data obtained causes little or no change in void fraction estimations after a point. Therefore, 300 ms test duration is considered for the test.

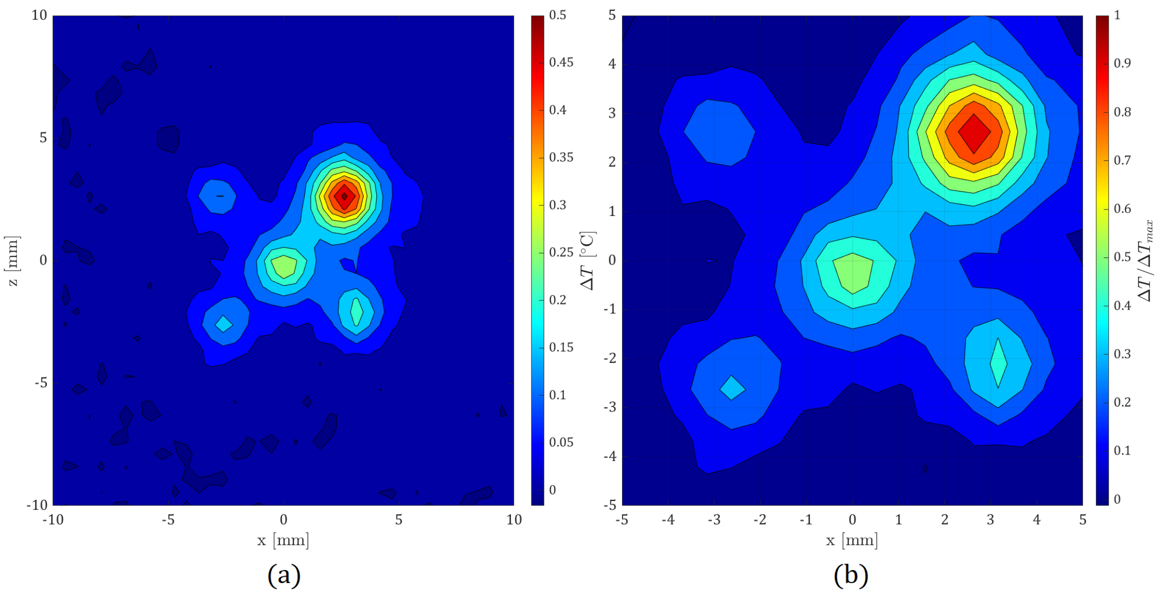

Figure 4.15. (a) The average temperature difference between the ideal TIM case and the synthetic measurements with $\sigma = 0.04$ °C, (b) zoomed and normalized temperature difference.

The initial guess choice plays a significant role in the inverse problem solution. As an initial guess, TIM is considered to be ideal, which means that there is no void within TIM (φ_g^0=0) for the simulations presented so far. An improved initial guess choice is investigated to decrease the number of iterations during void fraction distribution estimation and improve prediction accuracy. First, temperature measurements of IHS for the package with ideal TIM are calculated. A constant uniform die power of 90 W is applied for 300 ms to heat the package, and the simulated measurements are recorded with 10 ms intervals. Similarly, synthetic temperature measurements of IHS for the package with five voids are calculated by introducing normally distributed random measurement error with $\sigma = 0.04$ °C. The average temperature difference ΔT between the ideal TIM case and the synthetic measurements is illustrated in Figure 4.15 (a). It can be observed that the image at the center of Figure 4.15 (a) is similar to the actual void fraction distribution shown in Figure 4.4. In order to transform this information into an improved initial guess choice, the average temperature difference distribution illustrated in Figure 4.15 (a) is zoomed and normalized by dividing each temperature value by the maximum temperature value. The resulting distribution, which is to be used as an improved initial guess, is shown in Figure 4.15 (b).

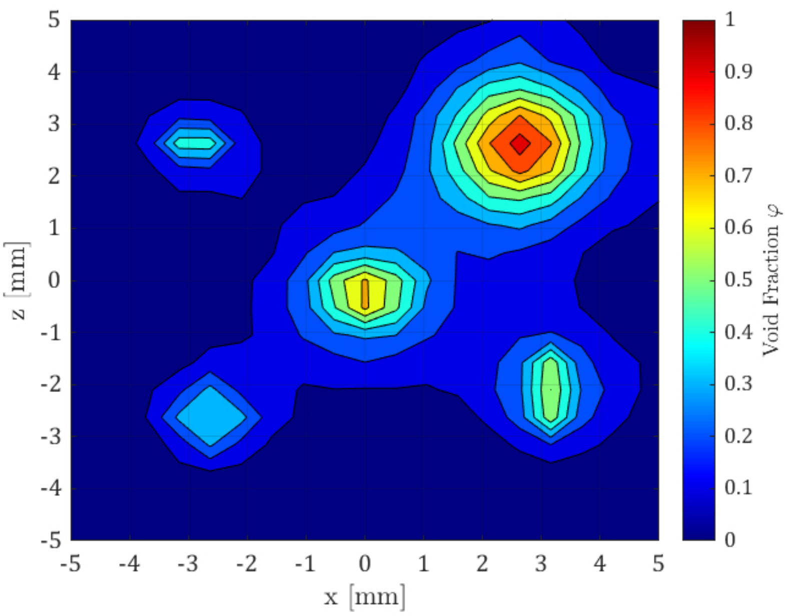

Figure 4.16. Ad-hoc filtered estimated void fractions in TIM using improved initial guess ($\sigma = 0.04$ °C).

Estimated void fraction distribution using the improved initial guess for synthetic measurement data with normally distributed random measurement errors with $\sigma = 0.04$ °C is illustrated in Figure 4.16. The average absolute error after the ad-hoc filtering is 0.11, whereas the maximum absolute error is 0.53 for the case shown in Figure 4.16. Although there is only a slight improvement in prediction accuracy, the number of iterations during void fraction distribution estimation decreased compared to the previous initial guess choice. Convergence is achieved in 14 iterations instead of 20 iterations as in the previous initial guess choice. Also, the estimated geometry and the size of Void 4 become more accurate, as shown in Figure 4.16.

The presented results indicate that the fuzzy inference method can estimate the void fraction distribution and identify the defects quantitatively by using IR measurements subject to random measurement error. The proposed method can even detect the smallest void, Void 4, reaching a void resolution of 0.05 mm^3. An IR imaging equipment with a normally distributed measurement error up to ± 0.12 °C is required with a 100 Hz measurement frequency to obtain the data used in this study, which is feasible with today's technology [53].

5. CONCLUSION

Tomography is a robust tool for the non-destructive characterization of systems utilized in a wide range of applications, from medical applications to materials science. Thermal tomography is a thermal imaging method that employs a thermal signal that diffuses into the characterized object. The diffusive character of the thermal signal makes accurate imaging a demanding problem. Due to the easy accessibility of thermal imaging devices, thermal tomography can present a cost-efficient and more feasible alternative to other imaging methods.

The feasibility of thermal tomography for the non-destructive characterization of defects in a flip chip package is studied numerically in this research. More precisely, the defects in thermal interface material layer that is referred to as TIM1 are identified since the flaws in TIM1 have a significant impact on the thermal performance of the package. The defects are modeled as voids whose properties are considered to be equal to the air properties in this study.

Thermal tomography application for quantitative defect characterization in a flip chip package faces two fundamental problems. The first one is the loss of thermal signal due to the nature of thermal diffusion and the heat spreading effect. The second one is the ill-posed nature of the thermal tomography problems, which means that the solution's existence, stability, and uniqueness might not be all satisfied. Therefore, the problem's solution is directly disturbed by the measurement error. The fuzzy inference method is used as an image reconstruction algorithm to handle these challenges.

The effect of voids in the thermal performance test is examined first to identify the size of the voids that have a noticeable impact on the temperature distribution of the package. Then, the thermal tomography test is performed to identify void locations and sizes.

In this study, the temperature measurement data, which is meant to be evaluated by experiments in Test-2, is simulated by solving the direct heat transfer problem for specified void fractions in TIM1 using the finite volume method with the implicit formulation. These simulated measurements are used to quantitatively characterize voids in TIM by estimating the void fractions using the fuzzy inference method. The results indicate that the void fraction estimation becomes considerably less accurate when a normally distributed random measurement error is introduced to simulated temperature measurements, especially when a measurement error with a standard deviation of $\sigma = 0.06$ °C is presented. Also, the results are out of the physically possible range of [0,1] for some of the sub volumes. Therefore, ad-hoc filtering is applied to resolve this problem.

Different test parameters are also investigated to find their effect on prediction accuracy and discover the proposed method's limits. Only minor improvements are observed as the die power is increased from 80 W to 90 W. 90 W die power is considered to be used in the test since there is almost no change in prediction accuracy when the die power used is increased from 90 W to 100 W. The effect of test duration on void fraction estimation is also investigated by comparing 100 ms, 300 ms, and 500 ms test duration. Results indicate that the geometry and the size of voids become more noticeable as the test duration is increased from 100 ms to 300 ms. The accuracy of the fuzzy inference method improves with increasing the number of images used. However, the increase in number of images obtained yields little or no change in void fraction estimations after a certain point. Therefore, 300 ms test duration is considered for the test. An improved initial guess choice is also investigated. The zoomed and normalized version of the temperature difference between the ideal TIM case and the synthetic measurements are calculated. It is used as an initial guess for the void fraction distribution, and the results indicate that the improved initial guess reduces the number of iterations by 30%.

It is possible to deduce that the fuzzy inference based thermal tomography offers great promise for non-destructive defect characterization in electronic packaging.

The suggested method requires IR equipment with a random measurement error up to ±0.12 °C with a 100 Hz measurement frequency. The main advantage of the proposed method is that it does not include the computationally demanding Jacobian calculation like other gradient-based optimization techniques. Thus, it can reach high grid resolutions with a less computational load than other gradient-based methods and detect voids as small as 0.05 mm^3. As a future work, the fuzzy inference method's validity can be investigated using experimental measurement data instead of simulated measurements. Also, the fuzzy inference method can be tested with different power maps instead of the uniform power map used in this study.

REFERENCES

1. Moore, G., “Cramming More Components onto Integrated Circuits, Reprinted from Electronics, volume 38, number 8, April 19, 1965, pp.114 ff”, *IEEE Solid-State Circuits Newsletter*, Vol. 11, pp. 33–35, 2006.

2. Erturk, H., “Non-Destructive Characterization of Multi Layer Objects by Thermal Tomography”, *ASME International Mechanical Engineering Congress and Exposition*, Vol. 9: Heat Transfer, Fluid Flows, and Thermal Systems, Parts A, B and C, pp. 2091–2100, 2009.

3. Gwinn, J. P. and R. L. Webb, “Performance and Testing of Thermal Interface Materials”, *Microelectronics Journal*, Vol. 34, No. 3, pp. 215–222, 2003.

4. Mukadam, M., J. Schake, P. Borgesen and K. Srihari, “Effects of Assembly Process Variables on Voiding at a Thermal Interface”, *The Ninth Intersociety Conference on Thermal and Thermomechanical Phenomena In Electronic Systems*, Vol. 1, pp. 58–62, 2004.

5. Pacheco, M., Z. Wang, L. Skoglund, Y. Liu, A. Medina, A. Raman, R. Dias, D. Goyal and S. Ramanathan, “Advanced Fault Isolation and Failure Analysis Techniques for Future Package Technologies”, *Intel Technology Journal*, Vol. 9, No. 4, pp. 337–352, 2005.

6. Gektin, V., “Thermal Management of Voids and Delamination in TIMs”, *International Electronic Packaging Technical Conference and Exhibition*, Vol. Advances in Electronic Packaging, Parts A, B, and C, pp. 641–645, 2005.

7. Chin, J. M., V. Narang, X. Zhao, M. Y. Tay, A. Phoa, V. Ravikumar, L. H. Ei, S. H. Lim, C. W. Teo, S. Zulkifli, M. C. Ong and M. C. Tan, “Fault Isolation in Semiconductor Product, Process, Physical and Package Failure Analysis: Impor-

tance and Overview", *Microelectronics Reliability*, Vol. 51, No. 9, pp. 1440–1448, 2011.

8. Huck, C., H. Zidek, T. Ebner, K. Wagner and A. Wixforth, "Liquid Crystal and Infrared Thermography on Coated SAW Devices", *2013 European Microwave Conference*, pp. 1423–1426, 2013.

9. Ross, R. J. (Editor), *Microelectronics Failure Analysis: Desk Reference*, ASM International, Ohio, 2011.

10. Aryan, P., S. Sampath and H. Sohn, "An Overview of Non-Destructive Testing Methods for Integrated Circuit Packaging Inspection", *Sensors*, Vol. 18, No. 7, pp. 1981–2018, 2018.

11. Zhang, G.-M., D. M. Harvey and D. R. Braden, "Microelectronic Package Characterisation Using Scanning Acoustic Microscopy", *NDT and E International*, Vol. 40, No. 8, pp. 609–617, 2007.

12. Khuri-Yakub, B. T., "Scanning Acoustic Microscopy", *Ultrasonics*, Vol. 31, No. 5, pp. 361–372, 1993.

13. Brosse, A., P. Naisson, H. Hamdi and J. Bergheau, "Temperature Measurement and Heat Flux Characterization in Grinding Using Thermography", *Journal of Materials Processing Technology*, Vol. 201, No. 1, pp. 590–595, 2008.

14. Kallis, J., G. Egan and M. Wirick, "Nondestructive Infrared Inspection of Hybrid Microcircuit Substrate-to-Package Thermal Adhesive Bonds", *IEEE Transactions on Components, Hybrids, and Manufacturing Technology*, Vol. 4, No. 3, pp. 257–260, 1981.

15. Lee, D.-H., "Thermal Analysis of Integrated-Circuit Chips Using Thermographic Imaging Techniques", *IEEE Transactions on Instrumentation and Measurement*, Vol. 43, No. 6, pp. 824–829, 1994.

16. Schmidt, C., C. Grosse and F. Altmann, "Localization of Electrical Defects in System in Package Devices Using Lock-in Thermography", *3rd Electronics System Integration Technology Conference ESTC*, pp. 1–5, 2010.

17. Gupta, A., Y. Liu, N. Zamora and T. Paddock, "Thermal Imaging for Detecting Thermal Interface Issues in Assembly and Reliability Stressing", *Thermal and Thermomechanical Proceedings 10th Intersociety Conference on Phenomena in Electronics Systems*, pp. 942–945, 2006.

18. Xu, Z., T. Shi, X. Lu and G. Liao, "Using Active Thermography for Defects Inspection of Flip Chip", *Microelectronics Reliability*, Vol. 54, No. 4, pp. 808–815, 2014.

19. Su, L., Z. Zha, X. Lu, T. Shi and G. Liao, "Using BP Network for Ultrasonic Inspection of Flip Chip Solder Joints", *Mechanical Systems and Signal Processing*, Vol. 34, No. 1, pp. 183–190, 2013.

20. Bakirov, V. F. and R. A. Kline, "Diffusion-Based Thermal Tomography", *Journal of Heat Transfer*, Vol. 127, No. 11, pp. 1276–1279, 2005.

21. Xu, Y., X. Wei and G. Wang, "Temperature-Change-Based Thermal Tomography", *International Journal of Biomedical Imaging*, Vol. 2009, 2009.

22. Sun, J., "Quantitative Three-Dimensional Imaging by Thermal Tomography Method", *AIP Conference Proceedings*, Vol. 1335, pp. 430–437, American Institute of Physics, 2011.

23. Swiderski, W., "The Characterization of Defects in Multi-Layered Composite Materials by Thermal Tomography Methods", *Proceedings of the Tenth Annual Conference of the Materials Research Society of Serbia*, Vol. 115, pp. 800–804, 2009.

24. Erturk, H., "Evaluation of Image Reconstruction Algorithms for Non-Destructive Characterization of Thermal Interfaces", *International Journal of Thermal Sci-*

ences, Vol. 50, No. 6, pp. 906–917, 2011.

25. Orlande, H. R., "Inverse Problems in Heat Transfer: New Trends on Solution Methodologies and Applications", *International Heat Transfer Conference*, Vol. 49439, pp. 379–398, 2010.

26. Shumakov, N., "A Method for the Experimental Study of the Process of Heating a Solid Body", *Soviet Physics-Technical Physics*, Vol. 2, No. 4, pp. 771–781, 1957.

27. Stolz, J., G., "Numerical Solutions to an Inverse Problem of Heat Conduction for Simple Shapes", *Journal of Heat Transfer*, Vol. 82, No. 1, pp. 20–25, 1960.

28. Alifanov, O. M., *Inverse Heat Transfer Problems*, Springer-Verlag, Berlin, 1994.

29. Tikhonov, A. N., "Solution of Incorrectly Formulated Problems and the Regularization Method", *Soviet Mathematics Doklady*, Vol. 4, pp. 1035–1038, 1963.

30. Bell, J. B., "Solutions of Ill-Posed Problems.", *Mathematics of Computation*, Vol. 32, No. 144, pp. 1320–1322, 1978.

31. Alifanov, O. M., "Solution of an Inverse Problem of Heat Conduction by Iteration Methods", *Journal of Engineering Physics*, Vol. 26, pp. 471–476, 1974.

32. Beck, J. V., B. Blackwell and C. R. S. Clair Jr, *Inverse Heat Conduction: Ill-Posed Problems*, Wiley, New York, 1985.

33. Siavashi, M., F. Kowsary and E. Abbasi, "Detection of Flaws in a Two-Dimensional Body through Measurement of Surface Temperatures and Use of Conjugate Gradient Method", *Computational Mechanics*, Vol. 46, pp. 597–607, 2010.

34. Huang, C. and M. Chaing, "A Thermal Tomography Problem in Estimating the Unknown Interfacial Enclosure in a Multiple Region Domain with an Internal Cavity", *Computer Modeling in Engineering and Sciences*, Vol. 53, No. 2, pp. 153–179,

2009.

35. Fan, C., F. Sun and L. Yang, “A General Quantitative Identification Algorithm of Subsurface Defect for Infrared Thermography”, *2005 Joint 30th International Conference on Infrared and Millimeter Waves and 13th International Conference on Terahertz Electronics*, Vol. 2, pp. 341–342, 2005.

36. Öner, B. and H. Ertürk, “Thermal Diffusion Tomography for Quantitative Non-Destructive Characterization of Electronic Packages”, *International Electronic Packaging Technical Conference and Exhibition*, Vol. 1: Thermal Management, 2015.

37. Divo, E., A. Kassab and F. Rodriguez, “An efficient singular superposition technique for cavity detection and shape optimization”, *Numerical Heat Transfer, Part B: Fundamentals*, Vol. 46, No. 1, pp. 1–30, 2004.

38. Kou, W., L. Chen, F. Sun and L. Yang, “Application of Bacterial Colony Chemotaxis Optimization Algorithm and RBF Neural Network in Thermal NDT/E for the Identification of Defect Parameters”, *Applied Mathematical Modelling*, Vol. 35, No. 3, pp. 1483–1491, 2011.

39. Wang, G., L. Zhu and H. Chen, “A Decentralized Fuzzy Inference Method for Solving the Two-Dimensional Steady Inverse Heat Conduction Problem of Estimating Boundary Condition”, *International Journal of Heat and Mass Transfer*, Vol. 54, pp. 2782–2788, 2011.

40. Zadeh, L., “Fuzzy Sets”, *Information and Control*, Vol. 8, No. 3, pp. 338–353, 1965.

41. Kalogirou, S. A., “Chapter 11 - Designing and Modeling Solar Energy Systems”, *Solar Energy Engineering*, pp. 583–699, Academic Press, Boston, 2nd edn., 2014.

42. Li, Y., G. Wang, H. Chen, Z. Zhu and D. Zhang, “A Decentralized Fuzzy Inference

Method for the Inverse Geometry Heat Conduction Problem", *Applied Thermal Engineering*, Vol. 106, pp. 109–116, 2016.

43. Wang, G., S. Wan, H. Chen, C. Lv and D. Zhang, "A Double Decentralized Fuzzy Inference Method for Estimating the Time and Space-Dependent Thermal Boundary Condition", *International Journal of Heat and Mass Transfer*, Vol. 109, pp. 302–311, 2017.

44. Wang, G., S. Wan, H. Chen, C. Lv and Q. Hua, "Fuzzy Estimation of Thermal Boundary Conditions of the Three-Dimensional Steady-State Heat Transfer System", *13th International Conference on Natural Computation, Fuzzy Systems and Knowledge Discovery*, pp. 1467–1473, 2017.

45. Wang, K., G. Wang, H. Chen, S. Wan and C. Lv, "Quantitative Identification of Three-Dimensional Subsurface Defect Based on the Fuzzy Inference of Thermal Process", *International Journal of Heat and Mass Transfer*, Vol. 133, pp. 903–911, 2019.

46. He, Y., "Rapid Thermal Conductivity Measurement with a Hot Disk Sensor: Part 2. Characterization of Thermal Greases", *Thermochimica Acta*, Vol. 436, No. 1, pp. 130–134, 2005.

47. Sahin, S. and S. G. Sumnu, *Thermal Properties of Foods*, pp. 107–155, Springer, New York, 2006.

48. Ozisik, M., *Heat Conduction*, Wiley, New York, 1980.

49. Sargolzaei, J., M. Khoshnoodi, N. Saghatoleslami and M. Mousavi, "Fuzzy Inference System to Modeling of Crossflow Milk Ultrafiltration", *Applied Soft Computing*, Vol. 8, No. 1, pp. 456–465, 2008.

50. Broekhoven, E. and B. De Baets, "Fast and Accurate Center of Gravity Defuzzification of Fuzzy System Outputs Defined on Trapezoidal Fuzzy Partitions", *Fuzzy*

Sets and Systems, Vol. 157, pp. 904–918, 2006.

51. Freitas, C. J., “The Issue of Numerical Uncertainty”, *Applied Mathematical Modelling*, Vol. 26, No. 2, pp. 237–248, 2002.

52. Roache, P. J., “Perspective: A Method for Uniform Reporting of Grid Refinement Studies”, *Journal of Fluids Engineering*, Vol. 116, No. 3, pp. 405–413, 1994.

53. Bhan, R. and V. Dhar, “Recent Infrared Detector Technologies, Applications, Trends and Development of HgCdTe Based Cooled Infrared Focal Plane Arrays and Their Characterization”, *Opto-Electronics Review*, Vol. 27, No. 2, pp. 174–193, 2019.

APPENDIX A: VERIFICATION OF FUZZY INFERENCE METHOD

Verification studies are carried out to compare the results to those reported in Wang *et al.* [39, 44] to ensure correct implementation of FIM for different problems. In the first study [39], FIM is used to estimate the unknown boundary temperature for a two-dimensional steady inverse heat conduction problem. A rectangular system with constant thermal properties is considered in the problem. The boundaries on the left and the top are assumed to be insulated, and there is a convection boundary condition on the right side. The boundary on the bottom maintains at a temperature function $f(x) = -2044x^2 + 613x + 100$ °C, which needs to be identified using temperature measurement points on the top. The finite difference method is applied to solve the direct heat conduction problem. The comparison of unknown boundary temperature estimation with $\sigma = 0.05$ °C standard deviation of the measurement error is shown in Figure A.1. The results show good agreement with the solution of Wang *et al.* [39] and the exact solution.

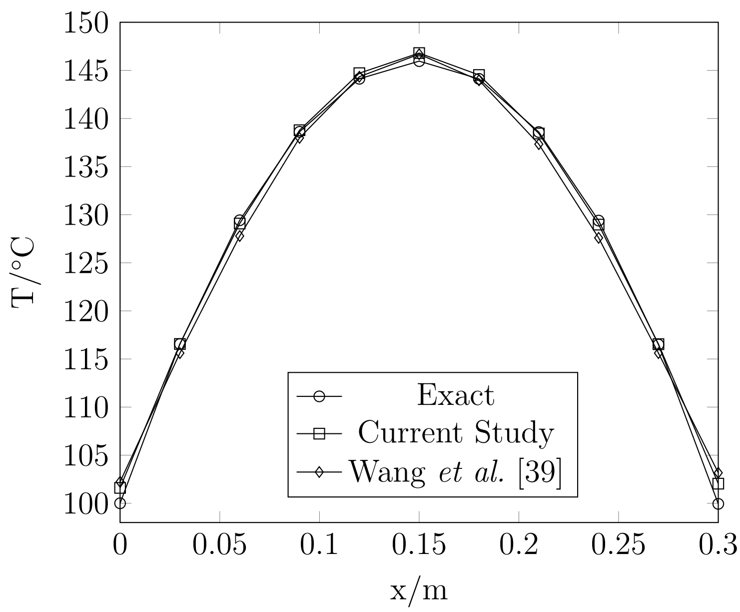

Figure A.1. Comparison of unknown boundary temperature estimation ($\sigma = 0.05$ °C).

Another verification study is carried out to test the accurate implementation of FIM for estimating unknowns when they are step functions. Wang *et al.* [44] utilized FIM to estimate the unknown heat flux distribution for a three-dimensional steady inverse heat conduction problem. A rectangular prism with constant thermal properties is considered in this problem. There is a convective heat transfer boundary condition on the right surface. The left surface of the plate is heated by a distributed heat flux $q(x, y)$, which needs to be identified using measured temperature at points on the right surface. The other four surfaces are insulated. The finite difference method is applied to solve the direct heat conduction problem. The exact distributed heat flux $q^{exa}(x, y)$ is given below:

$$q^{exa}(x,y) = \begin{cases} 2000 \text{ W/m}^2 & 0.5 < x < 1 \text{ m and } 0.5 < y < 1 \text{ m} \\ 0 \text{ W/m}^2 & \text{otherwise} \end{cases}, \tag{A.1}$$

where the comparison of unknown heat flux estimation with $\sigma = 0.1$ °C standard deviation of the measurement error is shown in Figure A.2. The results are in a good agreement with the solution of Wang *et al.* [44] and the exact solution. The permission for reuse of figures illustrated in Figure A.2 (a) and (b) is shown in Figure A.3.

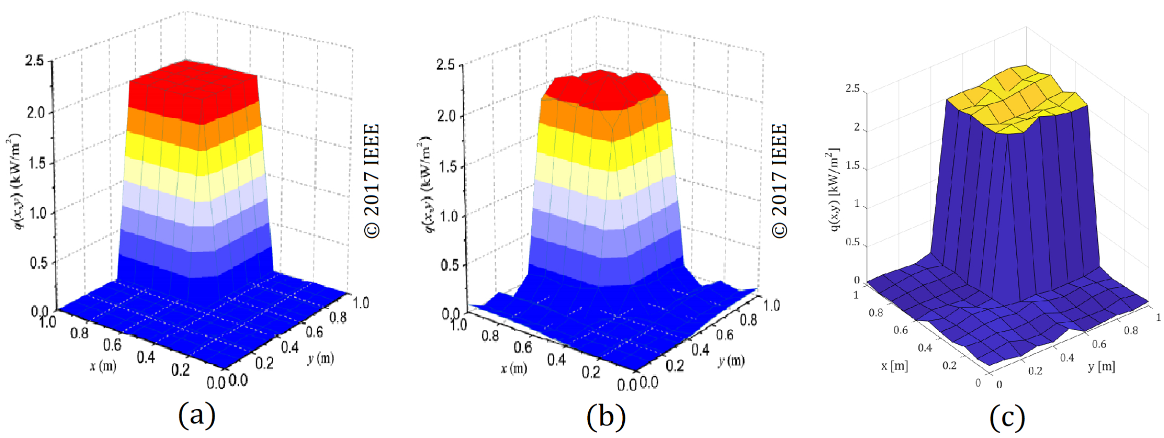

Figure A.2. (a) Actual heat flux, (b) estimated heat flux by Wang *et al.* [44], and (c) estimated heat flux by current study ($\sigma = 0.1$).

Fuzzy estimation of thermal boundary conditions of the three-dimensional steady-state heat transfer system

Conference Proceedings: 2017 13th International Conference on Natural Computation, Fuzzy Systems and Knowledge Discovery (ICNC-FSKD)
Author: Guangjun Wang
Publisher: IEEE
Date: July 2017

Thesis / Dissertation Reuse

The IEEE does not require individuals working on a thesis to obtain a formal reuse license, however, you may print out this statement to be used as a permission grant:

Requirements to be followed when using any portion (e.g., figure, graph, table, or textual material) of an IEEE copyrighted paper in a thesis:

1) In the case of textual material (e.g., using short quotes or referring to the work within these papers) users must give full credit to the original source (author, paper, publication) followed by the IEEE copyright line © 2011 IEEE.
2) In the case of illustrations or tabular material, we require that the copyright line © [Year of original publication] IEEE appear prominently with each reprinted figure and/or table.
3) If a substantial portion of the original paper is to be used, and if you are not the senior author, also obtain the senior author's approval.

Figure A.3. Permission for reuse of Figure A.2 (a) and (b).